Energy Transport and Relaxation in One-Dimensional Hamiltonian Systems

By

Suman G. Das

A thesis submitted to the Jawaharlal Nehru University
for the degree of Doctor of Philosophy

Department of Theoretical Physics
Raman Research Institute
Bangalore 560 080
April 2015

Typeset in LaTeX 2_ε.

Declaration:

I hereby declare that the work reported in this thesis is entirely original. This thesis is composed independently by me at Raman Research Institute under the supervision of Prof. Abhishek Dhar. I further declare that the subject matter presented in this thesis has not previously formed the basis for the award of any degree, diploma, membership, associateship, fellowship or any other similar title of any university or institution.

Prof. Abhishek Dhar

Suman Gaurab Das

Theoretical Physics Group
Raman Research Institute
Bangalore 560 080
India

Certificate:

This is to certify that the thesis entitled **"Energy Transport in One-Dimensional Hamiltonian Systems"** submitted by Suman Gaurab Das for the award of the degree of Doctor of Philosophy of Jawaharlal Nehru University is his original work. This has not been published or submitted to any other University for any other Degree or Diploma.

Prof. Ravi Subrahmanyan
(Centre Chairperson)
Director
Raman Research Institute
Bangalore 560 080
India

Prof. Abhishek Dhar
(Thesis Supervisor)

Acknowledgements

First and foremost I would like to thank my advisor Abhishek Dhar for his guidance throughout my Ph.D work. It is no overstatement to say that he has not only been a teacher and a collaborator, but a mentor whose views have significantly influenced my outlook on statistical physics.

I sincerely thank my friends and colleagues Anupam, Arnab, Prasad, Chaitra, Anjan, Mriganko, Madhuri, Vanitha and many others for the many hours spent in thoughtful discussions, not all of which included physics.

I thank Professors Sanjib Sabhapandit, Joseph Samuel, Supurna Sinha and other faculty at RRI for all that I learnt from them, and all manner of help and advice over the years.

Also, I thank my collaborators Onuttam Narayan, Keiji Saito, Herbert Spohn and Christian Mendl.

Special thanks to our group secretary Manjunath for making life easier at RRI. Thanks to the administration at RRI for all their help, technical and otherwise, which was invaluable to the completion of the thesis. Thanks to all the non-administrative staff as well for the wonderful support I received.

List of Publications and Preprints

I. Articles in journals:

[1] Suman G. Das, Abhishek Dhar, Keiji Saito, Christian B. Mendl, and Herbert Spohn. "Numerical test of hydrodynamic fluctuation theory in the Fermi-Pasta-Ulam chain." Physical Review E 90, no. 1 (2014): 012124.

[2] Suman G. Das, Abhishek Dhar, and Onuttom Narayan. "Heat Conduction in the $\alpha - \beta$ FermiPastaUlam Chain." Journal of Statistical Physics 154, no. 1-2 (2014): 204-213.

[3] Suman G. Das and Abhishek Dhar. "Landauer formula for phonon heat conduction: relation between energy transmittance and transmission coefficient." Eur. Phys. J. B 85, no. 11 (2012): 372.

II. Preprints:

[1] Suman G. Das, and Abhishek Dhar. "Role of conserved quantities in normal heat transport in one-dimenison." arXiv preprint arXiv:1411.5247 (2014).

Preface

This thesis deals with phononic energy transport in one-dimensional systems, both quantum and classical. The chief application is to the behavior of thermal conductivity in nanowires and nanotubes. We are primarily concerned with the question of anomalous versus normal energy transport in these systems. Normal transport refers to fluctuations that relax to equilibrium following the diffusion equation, for which well-defined transport coefficients exist. Anomalous diffusion, on the other hand, shows a more complicated mathematical behavior, and is characterized by diverging (or vanishing) transport coefficients. Energy diffusion in one-dimensional models is quite generally anomalous, though some specific conditions imposed on the model lead to normal transport. The central problem of this thesis is to understand and characterize anomalous transport properties of energy in one dimensional systems, and also to identify general criteria necessary for normal transport of energy. The problems addressed in various chapters of the thesis are briefly summarized below.

Chapter 1: Introduction

This chapter introduces the central problems and relevant literature.

Chapter 2: The Fermi-Pasta Ulam chain: Steady State and Thermal Conductivity

This chapter studies heat transport in the Fermi-Pasta-Ulam (FPU) chain, through nonequilibrium and equilibrium simulations, and for both symmetric and asymmetric inter-particle interactions. It identifies interesting finite-size effects and questions some previous results based on the use of the Green-Kubo formula for closed systems.

Chapter 3: Equilibrium Correlations and Hydrodynamics for the FPU Model

The spatiotemporal correlations of conserved fields in the FPU model is studied, and discussed in reference to the predictions of nonlinear fluctuating hydrodynamics. Implications for the heat conductivity are discussed, and connections with the nonequilibrium simulations of the previous chapter are made.

Chapter 4: Normal Heat Transport in the Coupled Rotator Model: Role of Conserved Quantities

The coupled rotator model is discussed as the exceptional case of a momentum-conserving model that shows normal transport, and fluctuating hydrodynamics is used to analyze and understand the model. As an outcome of the analysis, certain general hydrodynamic criteria for normal transport in one dimension are proposed.

Chapter 5: Exact Expression for Transmission Coefficients in Quantum Harmonic Lattices

An exact treatment of quantum harmonic lattices with arbitrary masses and spring constants connected to generalized Langevin baths is presented. In particular, an exact expression for transmissivity is given in terms of the transmission coefficients for individual frequencies. Both Lippmann-Schwinger scattering theory and direct solution of the wave equations are used to find transmission coefficients, and their equivalence is demonstrated.

Contents

1

Introduction

1.1 The problem of heat transport

The science of thermodynamics was developed in the eighteenth and nineteenth centuries as a description of the bulk properties of matter in equilibrium. Thermodynamics is phenomenological, and an attempt to understand the microscopic origins of the laws of thermodynamics led to the development of statistical mechanics in the late nineteenth and twentieth centuries. Although matter in equilibrium admits a simple and unified mathematical description, most interesting processes in the real world involve flow of mass, energy or charge. To understand these processes, phenomenological laws have been proposed and extensions of statistical mechanics have been made to explain nonequilibrium phenomena. As a general rule, dynamical properties exhibit less universality than static ones, and consequently nonequilibrium statistical mechanics has become a rich tapestry of theories, and the effort to understand transport phenomena continues to be

one of the major projects of physics. This thesis is primarily concerned with one particular topic of nonequilibrium physics - that of heat transport in one-dimensional systems with short-range interactions.

One of the oldest phenomenological laws of nonequilibrium physics is Fourier's law of heat transport. In one dimension it reads:

$$j = -\kappa \frac{\partial T}{\partial x}, \tag{1.1}$$

where j is the heat current, κ is the thermal conductivity, $T(x)$ is the local temperature. This is analogous to Ohm's law of electrical conduction, where an electrical current is proportional to the electrostatic potential gradient. However this superficial similarity hides an important difference - the electrostatic potential is a mechanical quantity that can be incorporated in a Hamiltonian, whereas temperature is an entropic quantity that emerges from a sufficiently chaotic dynamics at the microscopic scale. The existence of a local temperature is a necessary (but not sufficient) condition for the validity of Fourier's law, but there are no general theorems regarding the existence of local equilibrium in one dimension. On the contrary, there are simple models that explicitly show an absence of a local temperature. This gives an indication of the kind of problems associated with the microscopic modeling of heat transport phenomena.

The validity of Fourier's law is a central question in heat transport because Fourier's law implies normal transport of heat, whereas departure from Fourier's law signals anomalous transport. Normal transport means that energy fluctuations decay diffusively, i.e in accordance with the diffusion equation. The continuity equation for energy is $\partial_t e = -\partial_x j$, where e is the local energy density, assuming that heat flow is the only mechanism of energy transport. In combination with Fourier's law and the thermodynamic definition of specific heat density c_v, it gives

$$\frac{\partial T}{\partial t} = D \frac{\partial^2 T}{\partial x^2}, \tag{1.2}$$

where $D = \kappa / c_v$. Thus when a heat pulse is put into a specific point in the system at $t = 0$, the temperature profile at any later time t is a Gaussian centered about that point and with a variance $2Dt$. Since the continuity equation holds universally, Fourier's law is a necessary and sufficient condition for the normal diffusion of heat.

Typical nonequilibrium studies of heat transport attach heat baths at two different temperatures to the two ends of a one-dimensional lattice of size N, resulting in a steady heat current j. The

size-dependent conductivity is given as

$$\kappa(N) \equiv \frac{j\Delta T}{N} \tag{1.3}$$

where ΔT is the temperature difference between the two baths (it is important to that the temperature difference is smaller than the mean temperature of the baths, to ensure that the system is in the linear response regime). When Fourier's law holds, one expects that the system has a finite thermal conductivity in the large N limit, i.e the $Lim_{N\to\infty}\kappa(N)$ exists. What one finds more generally, however, is that the asymptotic behavior of κ is

$$\kappa \sim N^{\alpha} \tag{1.4}$$

where $0 \leq \alpha \leq 1$, and the exact value of α depends on the model. The case $\alpha = 0$ corresponds to a finite conductivity in the thermodynamic limit, and therefore to Fourier's law. However, as mentioned earlier, one should additionally check that local equilibrium exists in order to ensure that Fourier's law truly holds. When $\alpha > 0$, the diffusion equation no longer holds, and one requires an alternate description. There is good evidence that anomalous heat transport is characterized by Levy walks, and phenomenological Levy walk models of heat transport show reasonable agreement with molecular dynamics simulations.

This thesis studies phononic heat transport in one dimensional lattice models with nearest-neighbor couplings. The thesis builds on existing work, both old and recent, and a variety of analytical and numerical methods are used. The theory as described and developed here has direct ramifications for heat transport in nanowires and nanotubes, but also, hopefully, contributes in a more general way to the understanding of low-dimensional statistical mechanics.

The standard concepts, methods and theorems of statistical mechanics that are used throughout the thesis are outlined in the next section.

1.2 Basic concepts and theorems

1.2.1 The Langevin bath and the Einstein Relation

The effect of coupling of a system to a thermal environment is usually modeled through a stochastic heat bath, sometimes called a thermostat. There are several models of thermostats

available, but for this thesis we shall be using Langevin heat baths. For example, to numerically simulate the steady state of classical chains in Chapters 2 and 3, two ends of the system will be coupled to Langevin baths at two different temperatures.

The Langevin equation for the motion of a particle of mass m in a potential $U(x)$ is written as

$$m\frac{dv}{dt} + \gamma v = -U'(x) - \gamma v + \eta(t), \tag{1.5}$$

where γ is the coefficient of viscous friction and the thermal noise term η satisfies the statistical properties $\langle \eta(t) \rangle = 0$, and $\langle \eta(t)\eta(t') \rangle = D\delta(|t - t'|)\rangle$.

It can be shown that the equilibrium distribution of the particle follows the Gibbs formula provided that

$$D = 2\gamma k_B T, \tag{1.6}$$

where k_B is Boltzmann's constant. This result, often written in a slightly different form (owing to a different convention for defining D and γ), is called the Einstein relation. It can be extended in a straightforward way to many degrees of freedom with multiple noise and dissipation terms all corresponding to a thermal source at temperature T. Such a version of the theorem will be stated in Chapters 3 and 4.

1.2.2 The Fluctuation-Dissipation Theorem

Let x and y be two coordinates associated with a system, and let their correlation in equilibrium be

$$C_{xy}(t) \equiv \langle x(t)y(0) \rangle - \langle x \rangle \langle y \rangle. \tag{1.7}$$

From here on, angular brackets without subscripts denote equilibrium averages unless otherwise mentioned. Now consider an external field $f(t)$ turned on at time $t = 0$ that couples with x in the Hamiltonian in the form $f(t)x$. When $f(t)$ is small, the response of y to the field is given by

$$\langle y(t) \rangle_{ne} - \langle y \rangle = \int_0^t R_{xy}(t - t')f(t')dt' \tag{1.8}$$

where $\langle ... \rangle_{ne}$ denotes average over the non-equilibrium ensemble. $R_{xy}(t)$ is known as the response function. The fluctuation-dissipation theorem states that

$$\frac{d}{dt}C_{xy}(t) = k_B T R_{xy}(t). \tag{1.9}$$

This is one of the central results of linear response theory.

In the context of stochastic dynamics, it is possible to derive the Einstein relation from the fluctuation-dissipation theorem. In view of this, the Einstein relation is also sometimes called the (first) fluctuation-dissipation theorem.

1.2.3 The Green-Kubo formula

Transport coefficients can be related to the auto-correlation functions of the corresponding equilibrium current through the Green-Kubo formulas. We shall state here the Green-Kubo formula for the thermal conductivity κ.

$$\kappa = \frac{1}{k_B T^2} \lim_{\tau \to \infty} \lim_{L \to \infty} \frac{1}{L} \int_0^\tau dt \langle J(0) J(t) \rangle, \tag{1.10}$$

where $J(t)$ is the total heat current, and L is the system size. The ordering of the limits is important. The derivation of the formula assumes that the system is closed, and the formula is strictly valid only for finite transport coefficients, i.e when Fourier's law is valid. However, as we saw earlier, in one dimension one typically finds a diverging κ, and the usual method in such cases is to put the upper limit of the time integral at $\tau = L/c$, where c is the speed of sound, whereby a scaling of κ with L is obtained. This method is of a somewhat heuristic nature. However, there exists an exact Kubo-like formula for open systems of any size, and this is more suited to numerical simulations since it avoids any unexamined finite-size effects. This and other issues regarding the Green-Kubo formula will be further discussed in Chapter 2.

1.2.4 Local Thermal Equilibrium

Notice that the statement of Fourier's law, or indeed any mention of a temperature gradient, assumes the existence of a local temperature. This means that there must exist a length-scale much smaller than the system size such that the steady-state distribution of the particles

within that length is closely approximated by a Gibbs distribution with a suitably defined local temperature. This is the assumption of local thermal equilibrium, and is by no means easy to prove in a general case. In fact, lack of local thermal equilibrium has been explicitly demonstrated in certain models. Thus in non-equilibrium simulations one needs to verify the existence of local equilibrium, say by checking for the moments of the velocity distribution. This will be of relevance in Chapter 2 and will be discussed further there.

1.3 A Brief Overview of Early Results

One of the earliest investigations into the microscopic theory of heat transport was done by Reider, Lebowitz and Lieb [1]. They considered an ordered harmonic chain with two ends coupled to Langevin heat baths at two different temperatures. They obtained the exact steady state of the system, which is a multivariable Gaussian. The temperature profile was shown to be uniform with jumps at the boundaries, and the heat current was independent of the system size. This implies that the conductivity diverges as $\kappa \sim N$. The ballistic divergence is not surprising since in this problem all the normal modes are extended and non-interacting and thus heat is transported without scattering.

Mass-disordered harmonic chains were investigated by Casher and Lebowitz [2] and they showed that the system approaches a unique stationary state for a variety of baths. A landmark paper by Matsuda and Ishii [3] found that almost all modes in a disordered harmonic chain were exponentially localized, and at low frequencies the localization length for mode with frequency ω is proportional to $1/\omega^2$. This implies that for frequencies $\omega \sim 1/\sqrt{N}$ or less, the modes are essentially extended and can contribute to heat transport across the lattice. It has in fact been found that for free boundary conditions, the heat conductivity $\kappa \sim N^{1/2}$ for these systems. The conductivity, however, depends on boundary conditions and even spectral properties of baths. For example, for fixed boundary condition and white noise baths, the conductivity goes to zero as $N^{-1/2}$.

Attention soon turned to interacting systems, but relatively few rigorous analytical results are

available till date. In the main two different kinds of systems have been studied - momentum-conserving and momentum non-conserving systems. Momentum non-conservation is often implemented through pinning potentials at lattice sites. But there is also another model, that of the harmonic chain with random velocity flips, which has been worked out in considerable detail. Momentum non-conserving models show normal transport properties, with a converging conductivity at large system sizes.

Momentum conserving systems, however, tend to show anomalous conduction, with the conductivity diverging as $\kappa \sim N^{\alpha}$. A large number of numerical studies testify to this. However, there is considerable disagreement regarding the value of α, and even its universality for nonintegrable chains. A renormalization group-type calculation for systems at non-zero pressure was done in [18] and a universal exponent $\alpha = 1/3$ was predicted. A mode coupling theory developed in [5] made similar predictions. More recently, a theory of fluctuating hydrodynamics was developed for transport in one dimension by van Beijeren [6] and Spohn [7], which predict, among other more detailed results, that $\alpha = 1/3$ for anharmonic chains at non-zero pressure and $\alpha = 1/2$ at zero pressure. Contrary to this, previous simulations that were reported, for example, in [8], claim to find that anharmonic chains with asymmetric interaction potentials show normal transport at low temperatures and a transition to anomalous transport at high temperatures. Further, detailed numerical studies of the coupled rotator model, which is a momentum-conserving system, show clear signatures of normal transport. Thus, although certain approximate analytical results are available, the universality of these are not yet established, and several contradictory and even surprising results have been reported in the numerical literature.

1.4 Problems Addressed in the Thesis

We address, with varying degrees of success, the following problems in the thesis. We give a chapter wise summary of the problems treated.

1.4.1 Chapter 2

Does the heat conductivity exponent α for anharmonic chains depend on the nature of the anharmonic potential, or on the temperature? Recently, it has been suggested in [8], that one obtain normal transport at low temperatures for asymmetric interparticle potentials. This is in contradiction to results from previous mode-coupling theories. Are there any unusual finite-size effects that explain the results obtained in [8, 9] and other related works?

1.4.2 Chapter 3

The theory of nonlinear fluctuating hydrodynamics [7] predicted certain universal behavior for the spatiotemporal correlations of conserved fields in one-dimensional anharmonic chains. The theory has important implications for energy transport, but depends on a number of crucial approximations. To what extent do the predictions of the theory match with direct molecular dynamics simulations of the equilibrium correlations of anharmonic chains? How do these results tie up with the asymptotic scaling behavior of thermal conductivity?

1.4.3 Chapter 4

It has generally been believed that breaking translational invariance is crucial for normal heat transport in one dimension. However, an important counter-example in which normal transport has been observed is the chain of coupled rotators in one dimension. We realize that this model in fact belongs to a different universality class owing to the fact that it has less than three conserved fields. Can one use the theory of fluctuating hydrodynamics to understand energy transport in this model? What are the necessary and sufficient conditions for a one-dimensional classical model to exhibit normal heat transport?

1.4.4 Chapter 5

For quantum harmonic lattices with arbitrary parameters and coupled to generalized Langevin baths, we rigorously derive the Landauer formula, with an exact formal expression for the thermal conductivity. In particular, we relate the reflection and transmission coefficients of individual

modes to the energy transmissivity, using the Langevin Equation Green's Function (LEGF) as well as the boundary scattering approach.

2

The Fermi-Pasta-Ulam chain: Steady State and Thermal Conductivity

2.1 Introduction

One of the predictions from Fourier's law is about the scaling form of heat current J with system size N for a system with a fixed applied temperature difference. Fourier's law predicts $J \sim 1/N$ but for one dimensional $(1D)$ momentum conserving systems one typically finds:

$$J \sim \frac{1}{N^{1-\alpha}} \qquad \alpha > 0 \ . \tag{2.1}$$

In the linear response regime where a small temperature difference ΔT is applied, one can define the finite-size conductivity through the relation $\kappa = JN/\Delta T$. For anomalous systems one then expects the thermal conductivity to diverge with system size as $\kappa \sim N^{\alpha}$ [5, 7, 10, 18].

Determining the exact value of the exponent α and identifying universality classes has been an outstanding problem on which there is no consensus so far.

Two recent papers [8, 9] studied heat transport in several $1D$ models where the inter-particle interaction potential $V(x)$ is taken to be asymmetric, i.e $V(x) \neq V(-x)$. Based on nonequilibrium simulations as well as Green-Kubo formula-based equilibrium computations they conclude that, in certain parameter regimes, Fourier's law *is satisfied* in these systems, *i.e* for these systems κ converges to a size-independent value. This is a surprising result which raises a few questions: Do the analytical predictions based on mode-coupling theory and hydrodynamic arguments fail for asymmetric potentials? Zhong *et al* [8] find normal transport at low temperatures and anomalous transport at high temperatures. Is there a nonequilibrium phase-transition in this system as a function of temperature, or are finite size effects stronger at low temperatures, so that the true asymptotic (anomalous) behavior is only seen for much larger system sizes?

Section 2.2 considers the size-dependence of the conductivity at various temperatures and identifies important finite size-effects. Section 2.3 looks at other steady state properties such as temperature and thermal expansion profiles and substantiates these effects further. Section 2.4 looks at equilibrium heat current autocorrelations and connects them to behavior of the conductivity. Use of the usual closed-system Green-Kubo formula is shown to be problematic by comparing results from it to the conductivity obtained from direct non-equilibrium simulations as well as results from the open-systems Green-Kubo formula.

2.2 The Fermi-Pasta-Ulam Chain: Heat Current and Conductivity

We investigate the problem by studying a specific yet typical model of a nonlinear chain, the Fermi-Pasta-Ulam (FPU) model. This model is interesting in being one of the simplest nonlinear models about which a lot is known in the literature. Questions of zero-temperature dynamics as well as equilibration and transport have been studied in this model, and some contradictory claims and subtle issues are involved which will be discussed and addressed in due course. In this chapter we present a thorough numerical study of this model in a non-equilibrium ensemble, and

identify several interesting aspects of the finite-size behavior of conductivity.

The FPU model is described by the following Hamiltonian:

$$H = \sum_{l=1}^{N} \frac{p_l^2}{2m} + \sum_{l=1}^{N+1} [k_2 \frac{(q_l - q_{l-1})^2}{2} + k_3 \frac{(q_l - q_{l-1})^3}{3} + k_4 \frac{(q_l - q_{l-1})^4}{4}], \tag{2.2}$$

where $\{q_l, p_l\}$ denote the displacement about equilibrium lattice positions and momenta of particles. It is known from previous work in one-dimensional models that boundary conditions can have strong effect on the conductivity, and hence we consider and compare simulations with various boundary conditions. Fixed and free BCs are obtained by setting $q_0 = q_{N+1} = 0$ and $q_0 = q_1, q_N = q_{N+1}$ respectively. The interparticle harmonic spring constant is denoted by k_2 (which we set to 1) while $k_3,\ k_4$ denote the strengths of the cubic and quartic interactions respectively. To set up a heat current in this system the particles at the two ends of the chain are connected to stochastic white noise heat baths at different temperatures. The equations of motion of the chain are then given by:

$$\begin{aligned} m\ddot{q}_l = &-(2q_l - q_{l-1} - q_{l+1}) - k_3[(q_l - q_{l-1})^2 - (q_l - q_{l+1})^2] \\ &-k_4[(q_l - q_{l-1})^3 + (q_l - q_{l+1})^3] - \gamma_l \dot{q}_l + \eta_l \ , \end{aligned} \tag{2.3}$$

with $\eta_l = \eta_L \delta_{l,1} + \eta_R \delta_{l,N},\ \gamma_l = \gamma(\delta_{l,1} + \delta_{l,N})$. The noise terms satisfy the fluctuation dissipation relations $\langle \eta_L(t)\eta_L(t')\rangle = 2\gamma k_B T_L \delta(t-t')$, $\langle \eta_R(t)\eta_R(t')\rangle = 2\gamma k_B T_R \delta(t-t')$, k_B being Boltzmann's constant.

The energy current on the bond between particles l and $l+1$ is given by

$$j_l = \frac{1}{2}(\dot{q}_l + \dot{q}_{l+1})\ \partial H/\partial q_l \ . \tag{2.4}$$

We will mainly be interested in the ensemble-averaged heat current which is given by $\langle j \rangle = \sum_{l=1}^{N-1} \langle j_l \rangle / (N-1)$, where $\langle ... \rangle$ denotes a steady state average. For small temperature differences $\Delta T = T_L - T_R$, the current will vary linearly with ΔT and we define a size-dependent conductivity as

$$\kappa = \frac{N\langle j \rangle}{\Delta T} \ . \tag{2.5}$$

In general κ will be a function of $T = (T_L + T_R)/2$ and the parameters k_3, k_4. As noted in [11], Eqs. (2.3) are invariant under the transformation $T_{L,R} \to sT_{L,R}$, $\{q_l\} \to \{s^{1/2} q_l\}$ and $(k_3, k_4) \to$

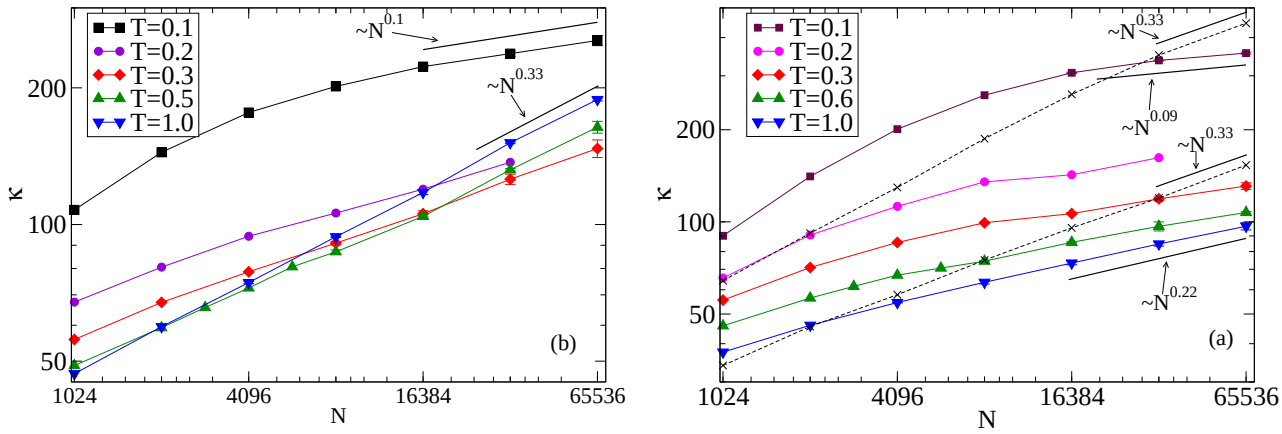

FIGURE 2.1: Plot of the conductivity κ versus system size in the FPU $\alpha - \beta$ model for (a)free and (b)fixed BCs at various values of the average temperature $T = (T_L + T_R)/2$ between 0.1 and 1.0. The parameters in the simulation were set at $k_2 = k_4 = 1$ and $k_3 = -1$. The dashed lines in (b) are results for the FPU β ($k_3 = 0$) model at temperatures $T = 0.1$ (upper curve) and $T = 1.0$.

$(k_3/s^{1/2}, k_4/s)$. This implies the scaling relation $J(T_L, T_R, k_3, k_4) = sJ(T_L/s, T_R/s, s^{1/2}k_3, sk_4)$. Defining the conductivity as in Eq. (2.5) we then get $\kappa(T, k_3, k_4) = \kappa(1, T^{1/2}k_3, Tk_4)$. In our study we keep k_3, k_4 fixed and study the effect of changing T. Note that increasing the temperature is equivalent to increasing both nonlinear terms in the interparticle potential, but the quartic term increases much faster, and so we expect any effect of an asymmetric potential to be more pronounced at low temperatures. This is borne out by our simulations.

The simplest way of determining the conductivity is through direct molecular dynamics (MD) simulation of the non-equilibrium steady state. In our simulations we used the velocity-Verlet algorithm with time steps $dt = 0.005$ [12]. We used $O(10^9)$ steps for relaxation and about the same number of steps for averaging. In our simulations we set $m = 1, \gamma = 1.0$, $k_2 = k_4 = 1$ and $k_3 = -1$ ((except where otherwise mentioned), with $T_L = T + \Delta T/2$ and $T_R = T - \Delta T/2$. We obtained data for $(T, \Delta T) = (1.0, 0.5), (0.5, 0.2), (0.3, 0.1), (0.2, 0.05), (0.1, 0.05)$. The size dependence of κ at these temperatures is plotted in Fig. (2.1) for fixed and free boundary conditions (BC).

For free BC, we see a clear anomalous behavior, $\kappa \sim N^{0.33}$, at high temperatures. As has

been observed in [8], the low temperature thermal conductivity seems to saturate at large system sizes. However, we see that the $\kappa(N)$ curves at intermediate temperatures ($T = 0.2, 0.3$ and 0.5) seem to flatten out in an intermediate range of N before turning around and increasing. At $T = 0.5, 1$ the curves seem to approach the asymptotic form $\kappa \sim N^{0.33}$, as has been predicted by certain previous studies. As the temperature is reduced, the intermediate-size effect becomes stronger rapidly: the flattening is barely noticeable for $T = 0.5$, while it is clear for $T = 0.3, 0.2$. For $T = 0.1$, one only sees a flattening of the $\kappa(N)$ curve, yielding a (substantially) smaller apparent α (it is more pronounced for fixed BC). Based on our observations for $T > 0.1$, we believe that this is because the large-N asymptotic regime has been pushed outside the size limit of our simulations. Note that if $\kappa(N)$ were to satisfy Fourier's law for large N, we would expect the flattened regime in the $\kappa(N)$ plots to broaden and move to the left as the temperature is lowered but with *no* subsequent turnaround, but this is not what is seen. Thus, although the asymmetry in the potential has greater impact at lower temperatures, we conjecture that the asymptotic scaling is temperature-independent.

The results for fixed BC as the temperature is varied are qualitatively similar, but with one difference - the flattening effect is much stronger, whereas the eventual approach to the anomalous scaling at large N is slower. Even the curve for $T = 1$ shows $\alpha < 0.33$. We note that this is probably because the additional scattering induced by pinning at the boundaries leads to a higher junction resistance, which is known to cause stronger finite-size effects.

2.3 Steady State Properties

We now examine other steady state properties. The temperature profile (defined as $T_l = m\langle \dot{x}_l^2 \rangle$) in the system gives some indication as to whether one is in the hydrodynamic regime. The temperature profiles for large N should collapse and jumps at the boundaries should be small. In Figs. (2.2,2.3) we plot the size dependence of temperature profiles for free and fixed BCs at low ($T = 0.1$) and high ($T = 1.0$) temperatures. In the insets we also plot the profile for the thermal expansion given by $\langle r_l \rangle = \langle q_{l+1} - q_l \rangle$. The most relevant observation from the temperature and expansion profiles is that at low temperatures, even at the largest system sizes, we do not see a collapse of the temperature profiles and this tells us that that the asymptotic regime has

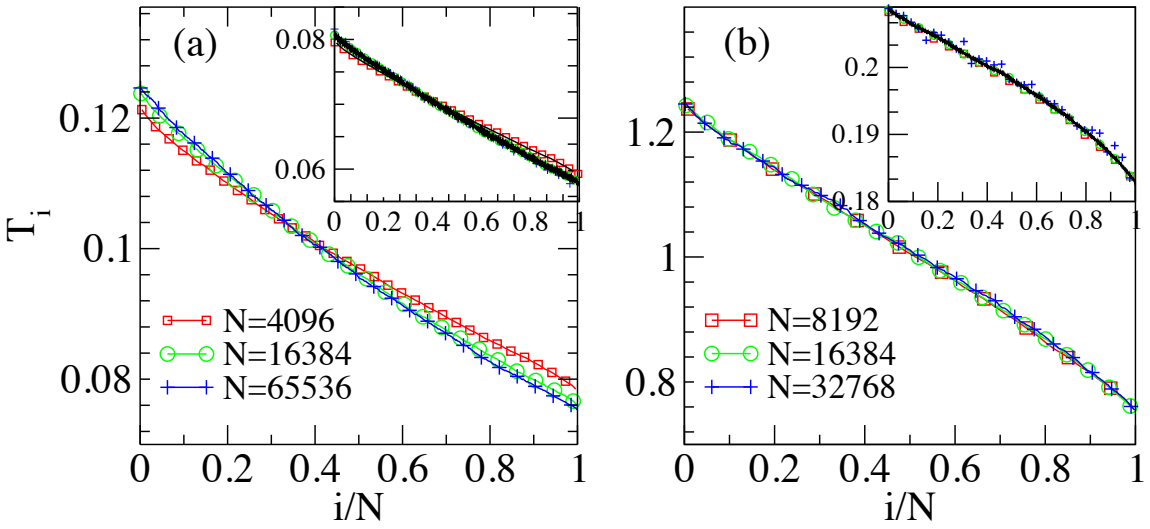

FIGURE 2.2: Plot of temperature profiles for different system sizes for free BC at temperatures (a) $T = 0.1$ and (b) $T = 1.0$. The insets show the expansion profile and the solid lines are from predictions assuming local thermal equilibrium.

not yet been reached. Secondly we see that for free BC the convergence is faster. Both these observations are consistent with our conclusions from the conductivity curves, that the change seen in the thermal conductivity of the system as the temperature is lowered does not reflect the asymptotic large-N behavior in this temperature regime.

We also compare the measured local expansion to the prediction from the measured local temperature and the assumption of local thermal equilibrium, to see if the assumption is valid. The local expansion can be obtained by assuming local thermal equilibrium and using the local temperature. For the case of free BC this is simple and the local expansion $\langle r_l \rangle$ is given by

$$\langle r_l \rangle = \frac{\int_{-\infty}^{\infty} dr_l \; r_l \; e^{-\beta_l V(r_l)}}{\int_{-\infty}^{\infty} dr_l \; e^{-\beta_l V(r_l)}} \; , \tag{2.6}$$

where $\beta_l = 1/T_l$. For the case of fixed BC the variables are not independent and we need impose the constraints $q_0 = q_{N+1} = 0$ or equivalently $q_0 = 0, \;\; \sum_{i=0}^{N} r_i = 0$. The local expansion is then given by

$$\langle r_l \rangle = \frac{\int_{-\infty}^{\infty} dr_0 \ldots \int_{-\infty}^{\infty} dr_N \; r_l \; e^{-\sum_l \beta_l V(r_l)} \; \delta(\sum_{j=0}^{N} r_j)}{\int_{-\infty}^{\infty} dr_0 \ldots \int_{-\infty}^{\infty} dr_N \; e^{-\sum_l \beta_l V(r_l)} \; \delta(\sum_{j=0}^{N} r_j)} \; .$$

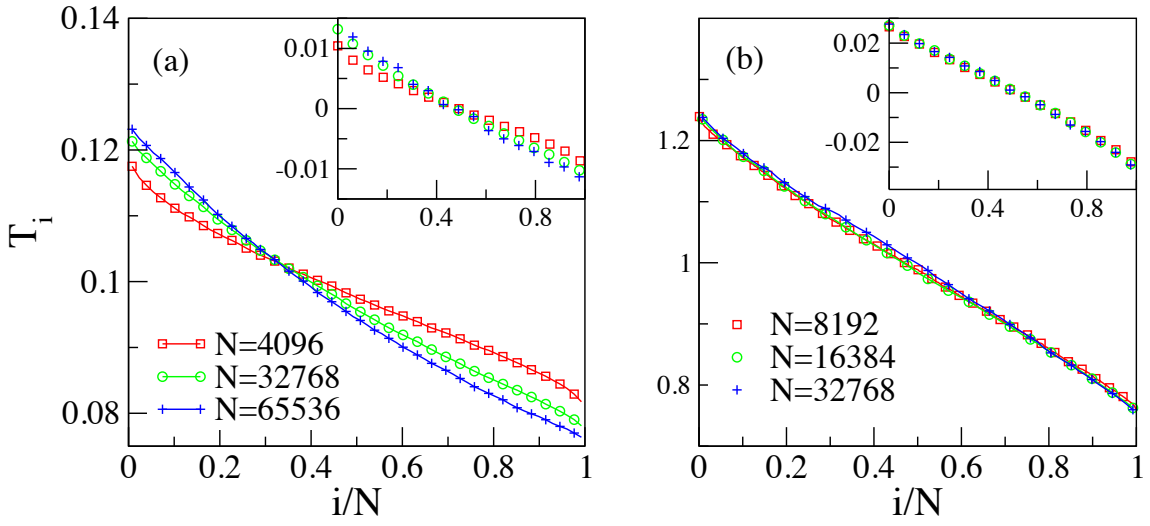

FIGURE 2.3: Plot of temperature profiles for different system sizes for fixed BCs at temperatures (a) $T = 0.1$ and (b) $T = 1.0$. The insets show the expansion profile.

Introducing the Fourier representation $\delta(y) = \int_{-\infty}^{\infty} dk e^{iky}/(2\pi)$ we then get

$$\langle r_l \rangle = \frac{\frac{1}{2\pi}\int_{-\infty}^{\infty} dk \prod_{j\neq l} \tilde{f}_j(k) \int_{-\infty}^{\infty} dr_l \; r_l \; e^{ikr_l} \; e^{-\beta_l V(r_l)}}{\frac{1}{2\pi}\int_{-\infty}^{\infty} dk \prod_j \tilde{f}_j(k)}, \tag{2.7}$$

where $\tilde{f}_j(k) = \int_{-\infty}^{\infty} dr_j e^{ikr_j} e^{-\beta_j V(r_j)}$. The solid black lines in the inset of Fig. (2.2) show the local equilibrium predictions for $\langle r_l \rangle$. For fixed BC it is difficult to evaluate Eq. (2.7) numerically for large system sizes, but for smaller sizes we find reasonable agreement with simulation results.

2.4 Thermal conductivity from linear response theory

The Green-Kubo formula relates transport coefficients of a system to the relevant equilibrium time correlation functions. For heat transport in one dimension, the Green-Kubo formula states

$$\kappa_{GK} = \lim_{\tau\to\infty} \lim_{N\to\infty} \frac{N}{k_B T^2} \int_0^{\tau} \langle j(0) j(t) \rangle dt, \tag{2.8}$$

where the current operator $j = \Sigma_1^N j_l/N$ and the angular brackets indicates an averaging over the initial equilibrium distribution. The time evolution is Hamiltonian. The order of the limits in Eq.(2.8) is important. κ_{GK} should be equal to $\lim_{\Delta T\to 0} \lim_{N\to\infty} \kappa$, where κ is defined by

Eq.(2.5). One also expects that the precise choice of boundary conditions in the evaluation of the correlation function should not matter in the thermodynamic limit.

Here we must advocate a word of caution regarding usage of the Green-Kubo formula for closed systems with initial conditions drawn from the canonical ensemble. It is essential while doing simulations to set the initial centre-of-mass momentum to zero for any particular trajectory of the system. If this is not done, then it can be shown that the correlations of the current J in the lab-frame is related to that of the current J_c in the centre-of-mass frame through

$$\langle J(0)J(t)\rangle \quad = \langle J_c(0)J_c(t)\rangle + NP^2/\beta, \tag{2.9}$$

where P is the pressure, and thus clearly the Green-Kubo formula gives a divergent conductivity due to the second term. See Appendix below for a derivation of the above relation.

For systems whose transport coefficients diverge in the thermodynamic limit – as is the case here – the limit $N \to \infty$ Eq.(2.8) does not exist. Typically the current-current correlation decays with a slow power law tail for an infinite system, giving a divergent conductivity. If instead one evaluates the integral on the right hand side of Eq.(2.8) for a finite system, it has been shown for a hard particle system [13] that the result is *qualitatively* different with periodic BC and with open BC connected to baths, calling into question any analysis that relies on periodic boundary conditions; this is because the tail of the correlation function is cut off differently in the two cases. For a chain, it is usual to set the upper cut-off in the Green-Kubo integral to $\sim N/c$, where c is the speed of sound, and thereby obtain the scaling of the conductivity (but not its exact magnitude). But this ad hoc procedure and has not been adequately justified in the literature.

As shown in [14], an exact Green-Kubo like linear response relation can be developed for open systems with the boundaries connected to heat baths. It relates the nonequilibrium κ to the equilibrium current autocorrelation decay in the following way:

$$\kappa = \lim_{\Delta T \to 0} \frac{N\langle j\rangle}{\Delta T} = \frac{N}{k_B T^2}\int_0^\infty \langle j(0)j(t)\rangle dt, \tag{2.10}$$

where the current operator now is $j = \Sigma_1^{N-1} j_{l,l+1}/(N-1)$. Formally Eq. (2.8) and Eq. (2.10) have the a similar structure but the correlation functions in the two cases are computed with different dynamics. Also, Eq. (2.10) is well-defined for finite N (in fact, it is exact for dynamics with Langevin heat baths), which is not the case for Eq. (2.8).

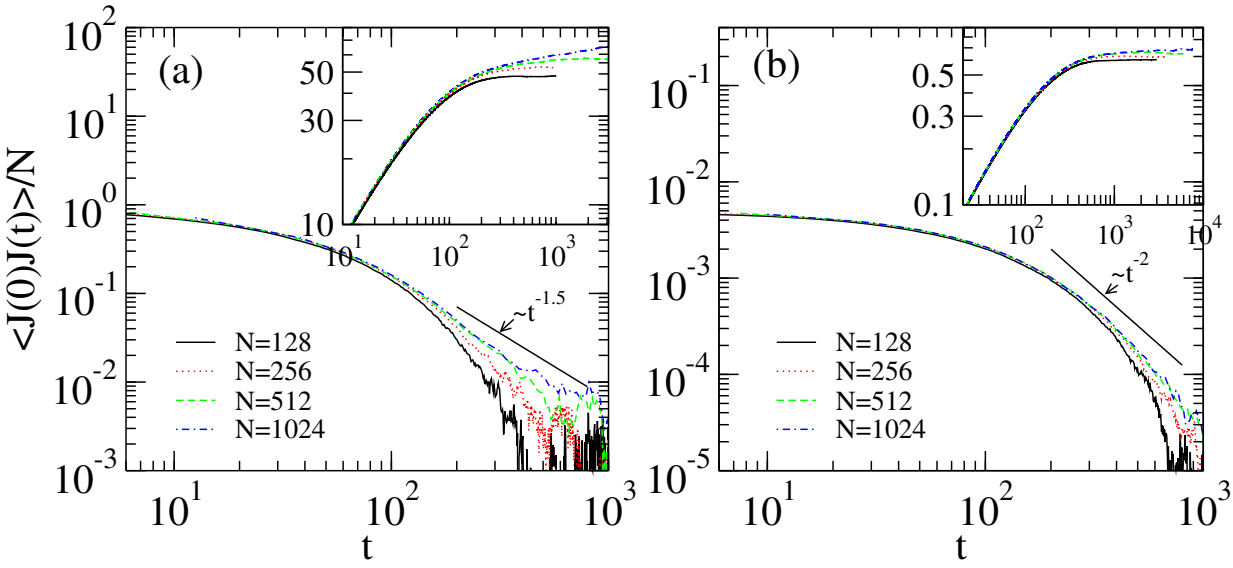

FIGURE 2.4: Plot of equilibrium current-current correlations using Hamiltonian dynamics for different system sizes at temperatures (a)$T = 0.1$ and (b)$T = 1.0$. The insets shows the integrated correlation function whose saturation value (divided by T^2) gives the thermal conductivity as defined by Eq (2.8). Periodic BCs were used in this simulation. In these simulations we set $k_3 = 2.0$.

We note that Ref. [9] and most simulations that use the Green-Kubo formula find the current auto-correlation for systems with periodic BCs. In view of the discussion above, we instead use heat bath dynamics and fixed BCs. The heat bath dynamics corresponds to Eqs. (2.3) with $T_L = T_R = T$. We also show the results for Hamiltonian dynamics with periodic BCs for comparison. In our simulations the system was initially equilibrated by connecting all points to Langevin type heat baths at the specified temperature. After equilibration, the heat baths were removed and the system was evolved using the two different dynamics. In the periodic BC case, for every initial condition, the center of mass momentum of the system was subtracted, as discussed before. We set the cubic anharmonicity to a larger value ($k_3 = 2.0$) in these simulations.

In Figs.(2.4) and (2.5), we show the structure of the heat current autocorrelation function in detail for Hamiltonian and heat bath dynamics respectively. Computing temporal correlation functions from simulations is numerically challenging, and we find that it is difficult to produce accurate data at larger system sizes. For the system sizes we can simulate, the form of the correlation functions for heat bath and Hamiltonian dynamics appear to be completely different. In the heat bath case with fixed BC we observe large oscillations in the correlation functions whose amplitude and period scale with system size. These correspond to sound modes which

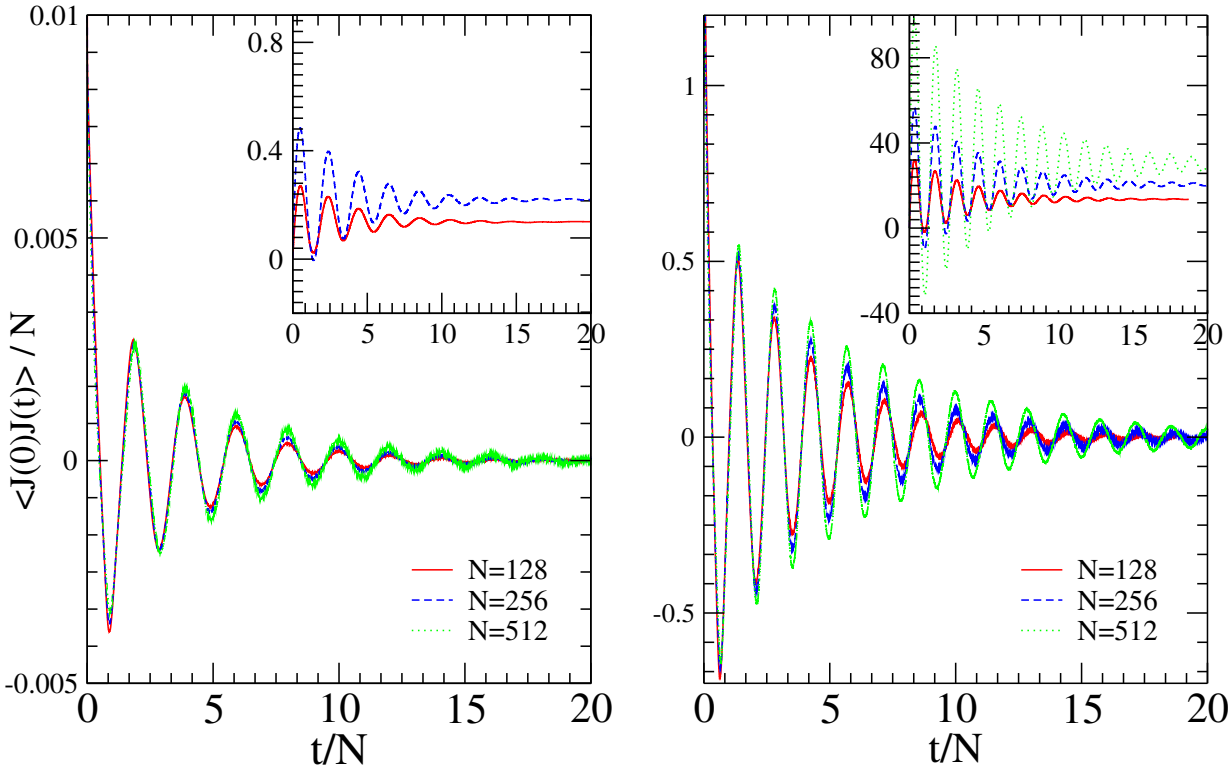

FIGURE 2.5: Plot of equilibrium current-current correlations using heat bath dynamics for different system sizes at temperatures (a)$T = 0.1$ and (b)$T = 1.0$. The insets show the integrated correlation function whose saturation value (divided by T^2) gives the thermal conductivity as defined by Eq (2.10). Fixed BCs were used in this simulation. In these simulations we set $k_3 = 2.0$.

are reflected at the boundaries. The periodic BC correlations do not show these oscillations and look very different. As has also been seen in [15] these, for some reason, seem to be very small in FPU models. Thus the difference between periodic and heat bath boundary conditions is even stronger than in Ref. [13]: not just the large-t cutoff but the form of the heat current autocorrelation function is different for the two cases. Thus, although we find that the heat current autocorrelation function decays rapidly as a function of time for periodic BC as in Ref. [9], this does not allow us to draw conclusions about the thermal conductivity. We note in passing that the tail of the autocorrelation function is $\sim t^{-1.5}$ in the low temperature plot, which is *slower* than the $\sim t^{-2}$ at high temperatures.

In Fig. (2.6) we plot the thermal conductivity obtained from the heat current autocorrelation function, both for Hamiltonian and heat bath dynamics, for different system sizes, and compare to the thermal conductivity directly obtained from nonequilibrium simulations. In the light of

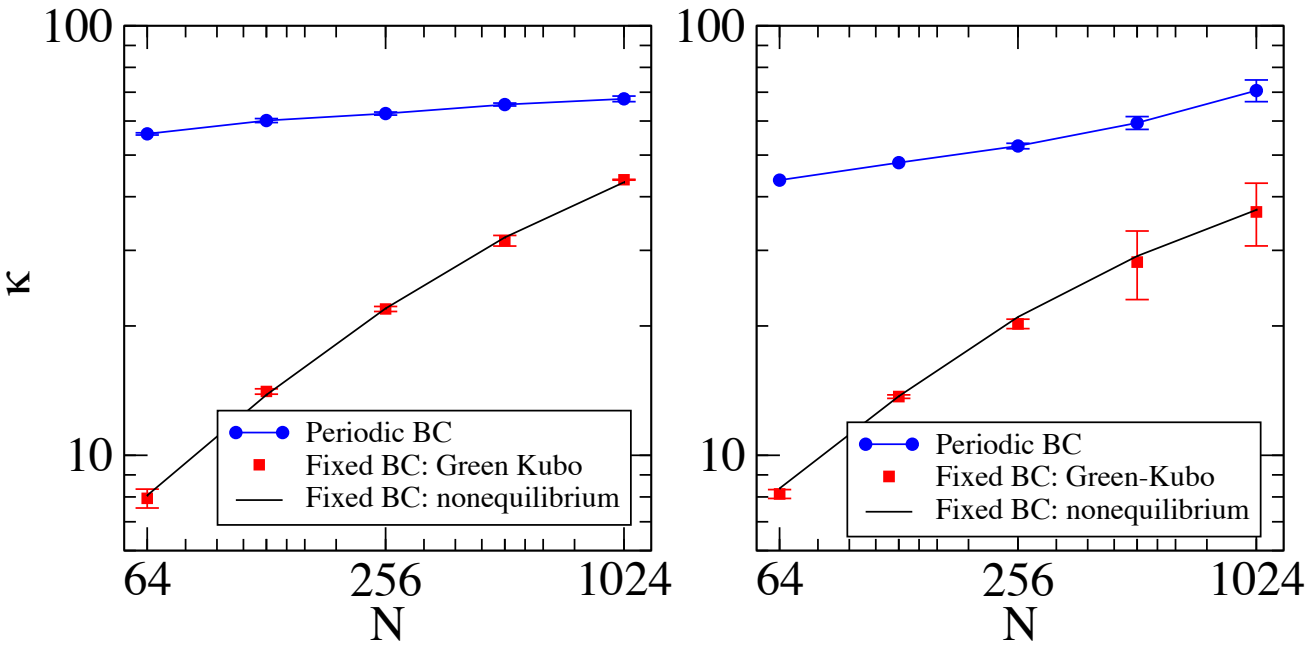

FIGURE 2.6: Comparison of the thermal conductivity obtained from the current-current correlation measurements of Figs. (2.4,2.5) and those obtained from direct nonequilibrium measurements for (a) $T = 0.1$ and (b) $T = 1.0$.

the discussion above, it is not surprising that the periodic BC case, which shows very weak N dependence, is quite different from the nonequilibrium results. The results with open BC and heat baths agree with the nonequilibrium results, as required by Eq.(2.10), but nonequilibrium simulations can be performed for much larger system sizes with relatively smaller error-bars. Therefore, we do not attempt to obtain the asymptotic large-N conductivity using the equilibrium Green-Kubo approach.

2.5 Conclusions

In this chapter, we provided numerical evidence to support the conclusion that the asymptotic large-N behavior of the thermal conductivity for (anharmonic) chains of particles does not depend on whether the interparticle potential is symmetric or asymmetric, contrary to recent suggestions [8, 9]. While the apparent thermal conductivity at low temperatures behaves differently for the sizes we have been able to simulate, the behavior as the temperature is tuned suggests

that this is due to insufficiently large system sizes. However, we are not able to completely rule out a phase transition in the system between diffusive and anomalous heat transport. We have also shown that computations based on the Green-Kubo formula have to be performed with the proper (i.e. heat bath) boundary conditions, in which case they agree with the results from our nonequilibrium simulations. Computing the Green-Kubo correlations is numerically more difficult, and one is restricted to smaller system sizes than for the nonequilibrium simulations.

It is an interesting question why, for the system sizes we are able to simulate, the heat conductivity at low temperatures differs so markedly from that at higher temperatures. In Refs. [8, 9], it is suggested that this may be due to inhomogeneous thermal expansion, which gives rise to an additional scattering mechanism that reduces the conductivity significantly (possibly due to the formation of localized modes). It is true that the hot and cold ends of the chain have different thermal expansion for asymmetric interparticle potentials, but this cannot affect the thermal conductivity in the linear response ($\Delta T \to 0$) regime: when ΔT is small, the variation in the local thermal expansion will be $O(\Delta T)$, and its impact on the heat current — which would be $O(\Delta T)$ for uniform thermal expansion — is $O(\Delta T^2)$. If the inhomogeneous thermal expansion *does* affect the measured thermal conductivity significantly, it indicates that the system is not simulated in the linear response regime (which, in our simulations, we have checked it is). Thus the observed finite-size effect cannot be understood in terms of non-uniform thermal expansion, and remains an open question.

APPENDIX

Let us consider a closed system of size N in equilibrium. The initial conditions for the dynamics are chosen from a canonical distribution, and the subsequent dynamics is Hamiltonian. Averages are taken over different realizations. The momenta of the individual particles satisfy the Maxwell-Boltzmann distribution, and the center-of-mass (COM) momentum $p_{cm} = \sum p_i/N$ has a Gaussian distribution with $\langle p_{cm}^2 \rangle = 1/(\beta N)$ (this is exact and follows from the properties of Gaussians).

Now the total current

$$J \equiv \sum j_i = \sum p_i f_{i-1,i} \tag{2.11}$$

where $f_{i-1,i}$ is the force on the i-th particle due to $(i-1)$-th particle. (One would expect that formally different but statistically equivalent definitions of current should obey the same analysis.)

One can re-write

$$p_i(t) = p_{cm} + p_{i,cm}(t), \tag{2.12}$$

where the first term on the r.h.s is the centre of mass momentum for any particular phase-space trajectory (corresponding to a specific set of initial conditions), and the second term is the momentum of each particle in the COM frame for that same trajectory. Since net momentum is conserved for a closed system, p_{cm} is constant. So the total current is now written as

$$J = p_{cm} \sum f_{i-1,i} + \sum p_{i,cm} f_{i-1,i} = p_{cm} P_{net} + J_c \tag{2.13}$$

where $P_{net} = \sum f_{i-1,i}$ is the net pressure. The local pressure is $P_i = f_{i-1,i}$. and the thermodynamic pressure is $P = \langle P_i \rangle = \langle P_{net} \rangle / N$. J_c is the heat current in the centre of mass frame. Using these relations,

$$\begin{aligned} \langle J(0)J(t) \rangle &= \langle J_c(0) J_c(t) \rangle \\ &+ \langle p_{cm} P_{net}(0) J_c(t) \rangle + \langle p_{cm} P_{net}(t) J_c(0) \rangle \\ &+ \langle p_{cm}^2 P_{net}(0) P_{net}(t) \rangle. \end{aligned} \tag{2.14}$$

We shall keep only terms $O(N)$ in the r.h.s in the thermodynamic limit, and drop higher-order corrections. Thus we can write $P_{net} = NP$ in the second, third and fourth terms, since fluctuations in P_{net} give terms $O(\sqrt{N})$. With this replacement, the second and third terms on the r.h.s now contain correlations like $\langle p_{cm}(t_1) J_c(t_2) \rangle$. Now the current J_c depends only on the initial momenta $p_{i,cm}$ in the COM frame and co-ordinates x_i. Further, in equilibrium the joint distribution of coordinates and momenta is separable into the product of the distributions for the center-of-mass momentum p_{cm}, the x_i and the $p_{i,cm}$ (with the distribution of the last one subject to the constraint $\sum p_{i,cm} = 0$, the constraint being independent of p_{cm}). Thus p_{cm} is uncorrelated to J_c, and $\langle p_{cm}(t_1) J_c(t_2) = 0 \rangle$. Thus one finally obtains

$$\begin{aligned} \langle J(0)J(t) \rangle &= \langle J_c(0) J_c(t) \rangle + \langle p_{cm}^2 \rangle N^2 P^2 \\ &= \langle J_c(0) J_c(t) \rangle + NP^2/\beta \end{aligned} \tag{2.15}$$

which is true in the thermodynamic limit at all times.

In the microcanonical ensemble restricted to the part of phase space with $p_{cm} = 0$, one should just see the first term, but in the canonical ensemble one should see both, even in the thermodynamic limit.

All this is valid for closed systems, for example Hamiltonian dynamics with free or periodic boundary conditions (this goes into the assumption of momentum conservation). In particluar, for the open-systems Green-Kubo formula discusssed in Chapter 1, equilibrium dynamics is stochastic and hence this derivation does not apply.

3

Equilibrium Correlations and Hydrodynamics for the FPU Model

3.1 Introduction

While non-equilibrium studies and equilibrium current auto-correlations directly give the thermal conductivity of a system, a systematic analytical approach to anomalous transport in those areas is lacking. On the other hand, one-dimensional hydrodynamics has been developed in a more thorough way and some universal predictions for equilibrium spatiotemporal correlations exist. These can be used to understand thermal transport.

In this chapter we perform direct molecular dynamics simulations of the Fermi-Pasta-Ulam chain to compute various spatiotemporal correlation functions and compare them with the predictions from hydrodynamics. This helps us establish connections with thermal conductivity exponents.

Section 3.2 summarizes the scaling predictions of fluctuating hydrodynamics for more details see [7]. Section 3.3 presents results from the simulation of the FPU model in various temperature and pressure regimes, as well as with symmetric and asymmetric interparticle interactions, and discusses agreements and disagreements with the predictions from hydrodynamics. The salient points are summarized in Section 3.4.

3.2 Predictions of nonlinear fluctuating hydrodynamics

Apart from direct simulations of the steady state of a one-dimensional system, the thermal conductivity can be found by using the Green-Kubo formula through the integral of the equilibrium heat current auto-correlation function. Simulations and several theoretical approaches [6, 17–22] find that the correlation function has a slow power law decay $\sim 1/t^{1-\alpha}$ and this gives a divergent conductivity. A number of papers [13, 23–29] have studied the decay of equilibrium energy fluctuations or of heat pulses and find that they show super-diffusion. This has been understood through phenomenological models in which the energy carriers perform Levy walks [25–28]. A significant step towards understanding anomalous heat transport in one-dimension was achieved in [6, 7], where a detailed theory of hydrodynamic fluctuations in anharmonic chains has been developed and several analytical results obtained. The main power of this theory is that it is able to make very detailed predictions that can be verified through direct simulations of microscopic models. Unlike earlier studies which have mainly focused on the thermal conductivity exponent α, the hydrodynamic theory predicts the scaling forms of various correlation functions, including prescriptions to compute various parameters for given microscopic models. The hydrodynamic theory naturally has to make various assumptions to arrive at the results and hence there is a need to perform direct molecular dynamic simulations that can check the theory. A recent paper [16] has presented results for such a test for the case of a hard particle gas interacting via the so-called shoulder potential. Here we consider the Fermi-Pasta-Ulam (FPU) chain as a typical anharmonic model and report simulation results on equilibrium correlations in different parameter regimes. Implications for thermal conductivity exponents are discussed in detail.

We first summarize the results of the theory in [7]. Consider N particles with position and momenta described by the variables $\{q(x), p(x)\}$, for $x = 1, \ldots, N$, and moving on a periodic

ring of size L such that $q(N+1) = q(1) + L$ and $p(N+1) = p(1)$. Defining the extension variables $r(x) = q(x+1) - q(x)$, we consider the system to have the following Hamiltonian with nearest neighbor interactions

$$\begin{aligned} H &= \sum_{x=1}^{N} \epsilon(x), \\ \text{where } \epsilon(x) &= \frac{p^2(x)}{2} + V[r(x)] \ , \end{aligned} \tag{3.1}$$

where the particles have been taken to have unit masses. From the Hamiltonian equations of motion one sees that the extension $r(x)$, momentum $p(x)$ and energy $\epsilon(x)$ are locally conserved quantities satisfying the following equations of motion

$$\begin{aligned} \frac{\partial r(x,t)}{\partial t} &= \frac{\partial p(x,t)}{\partial x}, \\ \frac{\partial p(x,t)}{\partial t} &= -\frac{\partial P(x,t)}{\partial x}, \\ \frac{\partial e(x,t)}{\partial t} &= -\frac{\partial}{\partial x}[p(x,t)P(x,t)] \ , \end{aligned} \tag{3.2}$$

where $P(x) = -dV(r)/dr|_{x-1}$ is the pressure and $\partial f/\partial x = f(x+1) - f(x)$ denotes the discrete derivative. Suppose the system is in a state of thermal equilibrium described by zero total average momentum and where the average energy and expansion are respectively fixed by specifying the temperature ($T = \beta^{-1}$) and pressure (P) of the system. This corresponds to an ensemble described by the distribution

$$\begin{aligned} \mathcal{P}(\{p(x), r(x)\}) &= \prod_{x=1}^{N} \frac{e^{-\beta[p_x^2/2 + V(r_x) + P r_x]}}{Z_x} \ , \\ \text{where } Z_x &= \int_{-\infty}^{\infty} dp \int_{-\infty}^{\infty} dr e^{-\beta[p^2/2 + V(r) + Pr]} \ . \end{aligned} \tag{3.3}$$

Now consider small fluctuations of the conserved quantities about the equilibrium values $u_1(x,t) = r(x,t) - \langle r \rangle_{eq}$, $u_2(x,t) = p(x,t)$ and $u_3(x,t) = \epsilon(x,t) - \langle \epsilon \rangle_{eq}$. The fluctuating hydrodynamic equations for the field $u = (u_1, u_2, u_3)$ is now written by expanding the conserved currents in Eq. (3.2) to second order in the nonlinearity and then adding dissipation and noise terms to ensure thermal equilibration. One then gets the hydrodynamic equations

$$\partial_t u_\alpha = -\partial_x \left[A_{\alpha\beta} u_\beta + H^{\alpha}_{\beta\gamma} u_\beta u_\gamma - \partial_x \widetilde{D}_{\alpha\beta} u_\beta + \widetilde{B}_{\alpha\beta} \xi_\beta \right] \ . \tag{3.4}$$

The noise and dissipation matrices $(\widetilde{B}, \widetilde{D})$ are related by the fluctuation-dissipation relation $\widetilde{D}C + C\widetilde{D} = \widetilde{B}\widetilde{B}^T$, where the matrix C corresponds to equilibrium correlations and has elements $C_{\alpha\beta}(x) = \langle u_\alpha(x,0)u_\beta(0,0)\rangle$.

Neglecting the nonlinear terms, we move to the normal modes of the linearized equations by effecting the transformation $(\phi_{-1}, \phi_0, \phi_1) = \phi = Ru$, where the matrix R diagonalizes A, *ie.,* $RAR^{-1} = \mathrm{diag}(-c, 0, c)$. The diagonal form implies that there are two sound modes $(\phi_\pm)$ traveling at speed c in opposite directions, and one stationary but decaying heat mode (ϕ_0). Next one solves the nonlinear hydrodynamic equations within mode-coupling approximation and makes predictions for the equilibrium spatiotemporal correlation functions $C_{ss'}(x,t) = \langle \phi_s(x,t)\phi_{s'}(0,0)\rangle$, where $s, s' = -, 0, +$. For the generic case of non-zero pressure, (i.e $P \neq 0$), which corresponds either to asymmetric inter-particle potentials or to externally applied stress, the prediction for the left-moving sound mode and the heat mode are respectively

$$C_{--}(x,t) = \frac{1}{(\lambda_s t)^{2/3}}\ f_{KPZ}\left[\ \frac{(x+ct)}{(\lambda_s t)^{2/3}}\ \right]\ , \tag{3.5}$$

$$C_{00}(x,t) = \frac{1}{(\lambda_e t)^{3/5}}\ f_{LW}^{5/3}\left[\ \frac{x}{(\lambda_e t)^{3/5}}\ \right]\ , \tag{3.6}$$

where $f_{KPZ}(x)$ is the KPZ scaling function discussed in [7, 30], and tabulated in [31]. $f_{LW}^{\nu}(x)$ is the Fourier transform of the Levy characteristic function $e^{-|k|^\nu}$. For the special case $P = 0$, the corresponding quantities are:

$$C_{--}(x,t) = \frac{1}{(\lambda_s^0 t)^{1/2}} f_G\left[\ \frac{(x+ct)}{(\lambda_s^0 t)^{1/2}}\ \right]\ , \tag{3.7}$$

$$C_{00}(x,t) = \frac{1}{(\lambda_e^0 t)^{2/3}}\ f_{LW}^{3/2}\left[\ \frac{x}{(\lambda_e^0 t)^{2/3}}\ \right]\ . \tag{3.8}$$

where $f_G(x)$ is the unit Gaussian with zero mean.

For the non-zero pressure case, the scaling coefficients λ_s and λ_e for the sound and heat mode respectively are given by

$$\lambda_s = 2\sqrt{2}|G_{11}^1|, \lambda_e = {\lambda_s}^{-2/3} C^{-1/3} (G_{11}^0)^2 a_e, \tag{3.9}$$

where $a_e = 2\sqrt{3}\,\Gamma(1/3)\int_{-\infty}^{\infty}\ dx f_{KPZ}(x)^2 = 3.167...$ is a model-independent numerical constant, and the matrices G^α are related to the nonlinear coupling matrices H^α through the normal mode transformation effected by R (see Appendix for details).

For the case of zero pressure, λ_s^0 depends on the coefficients of the noise and dissipation terms introduced in Eq. 4.1, and since all of the coefficients are not simultaneously determined by the temperature and the fluctuation-dissipation relations, λ_s^0 remains undetermined by the theory. The scaling coefficient for the heat mode in this case is

$$\lambda_e^0 = (\lambda_s^0)^{-1/2} c^{-1/2} (G_{11}^0)^2 (4\pi)^2 a_e^0, \tag{3.10}$$

where $a_e^0 = 4 \int_0^\infty dt\ t^{-1/2} cos(t) \int_{-\infty}^\infty dx\ f_G(x)^2 = \sqrt{2}$. A simulation of the microscopic dynamics can be used to find λ_s^0, and from there one can calculate λ_e^0 using the above formula.

In the following section, we discuss the results of our molecular dynamics simulations to compute the correlation functions and compare them with the scaling predictions.

3.3 Molecular Dynamics Simulations

We consider the FPU $\alpha - \beta$ model described by the following inter-particle potential

$$V(r) = k_2 \frac{r^2}{2} + k_3 \frac{r^3}{3} + k_4 \frac{r^4}{4}\ . \tag{3.11}$$

The set of variables $\{r(x), p(x)\}$ are evolved according to the equations of motion

$$\dot{r}(x) = p(x+1) - p(x), \quad \dot{p}(x) = V'(r(x)) - V'(r(x-1))\ , \tag{3.12}$$

for $x = 1, 2, \ldots, N$ and with initial conditions chosen from the distribution given by Eq. (3.3). The product measure means that it is easy to generate the initial distribution directly and one does not need to dynamically equilibrate the system. The integrations have been done using both the velocity-Verlet algorithm [12] and also through the fourth order Runge-Kutta algorithm and we do not find any significant difference. The full set of two-point correlation functions were obtained by averaging over around $10^6 - 10^7$ initial conditions. Here we present results for four different parameter sets.

Set I: $k_2 = 1.0, k_3 = 2.0, k_4 = 1.0, T = 0.5, P = 1.0$. These are the set of parameters used in [16] for the numerical solutions of the mode-coupling equations. In Fig. (3.1) we show the heat mode correlation C_{00} and the sound mode correlations C_{--}, C_{++} at three different times. The speed of sound is $c = 1.45468...$ The dotted vertical lines in the figure indicate the distances

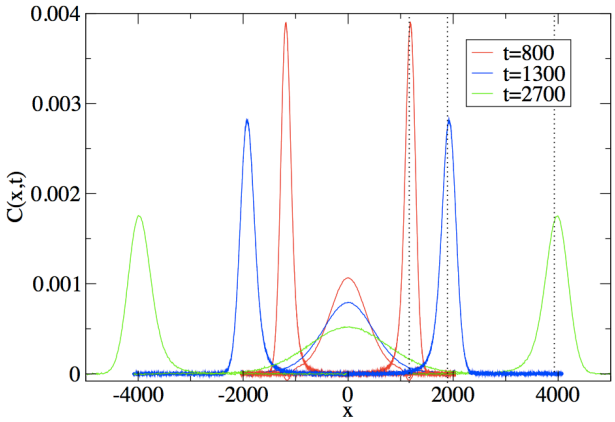

FIGURE 3.1: Set I: Correlation functions for the heat mode and the two sound modes at three different times. At the latest time we see that the heat and sound modes are well separated. The parameters of the simulation are $k_2 = 1,\ k_3 = 2,\ k_4 = 1,\ T = 0.5$ and $P = 1$. The speed of sound is $c = 1.45468$ and the system size was $N = 8192$.

$\ell = ct$. The sound peaks are at their anticipated positions. In Fig. (3.2) we show the heat mode and the left moving sound mode after scaling according to the predictions in Eqs. (3.5,3.6). One can see that the scaling is excellent. For comparison we have also plotted a Lévy-stable distribution and the KPZ scaling function [31], and find that the agreement is good for the heat mode but not convincing for the sound mode. One observes a significant asymmetry in the sound mode correlations, contrary to what one would expect from the symmetric KPZ function.

From our numerical fits shown in Fig. (3.2) we obtain the estimates $\lambda_s = 2.05$ and $\lambda_e = 13.8$. The theoretical values based on Eq. (3.9) are $\lambda_s = 0.675$ and $\lambda_e = 1.97$ (see Appendix), which thus deviates significantly from the numerical estimates obtained from the simulations. The disagreement could mean that, for this choice of parameters, we are still not in the asymptotic hydrodynamic regime. We expect that the scaling will improve if the heat and sound mode are more strongly decoupled. To check this, we simulated a set of parameters where the sound speed is higher and the separation between the sound and heat modes is more pronounced. We now discuss this case.

Set II: $k_2 = 1.0, k_3 = 2.0, k_4 = 1.0, T = 5.0, P = 1.0$. This choice of parameters gives $c = 1.80293$ and we see in Fig. (3.4) there is much better separation of the heat and sound modes. We again find an excellent collapse of the heat mode and the sound mode data with the expected scalings in Fig. (3.5) . The heat mode fits very well to the Lévy-scaling function.

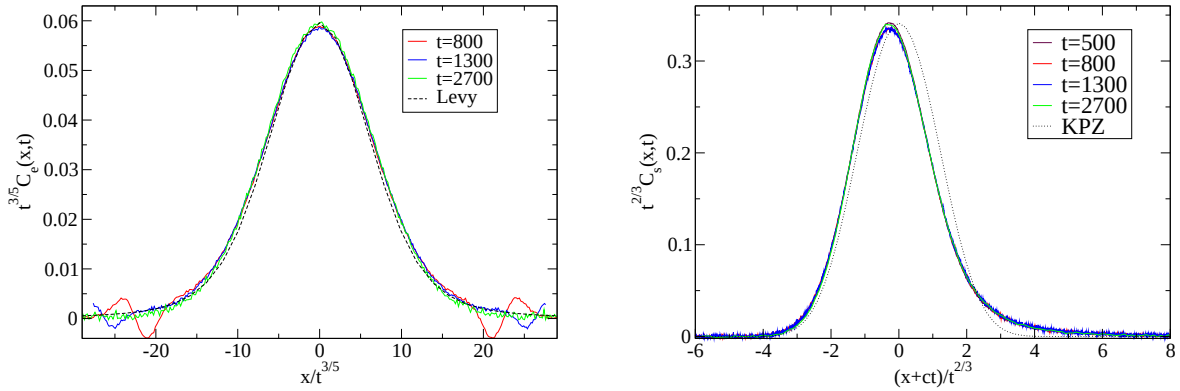

Figure 3.2: Set I: Scaled plots of heat mode and left moving sound mode correlations, at different times, using a Levy-type-scaling for the heat mode and KPZ-type scaling for the sound mode. The parameters in the simulation were $k_2 = 1, k_3 = 2, k_4 = 1, T = 0.5, P = 1.0$ and $N = 8192$. We see here that the collapse of different time data is very good. The fit to the Levy-stable distribution with $\lambda_e = 13.8$ is quite good, while the fit to the KPZ scaling function with $\lambda_s = 2.05$ is not convincing.

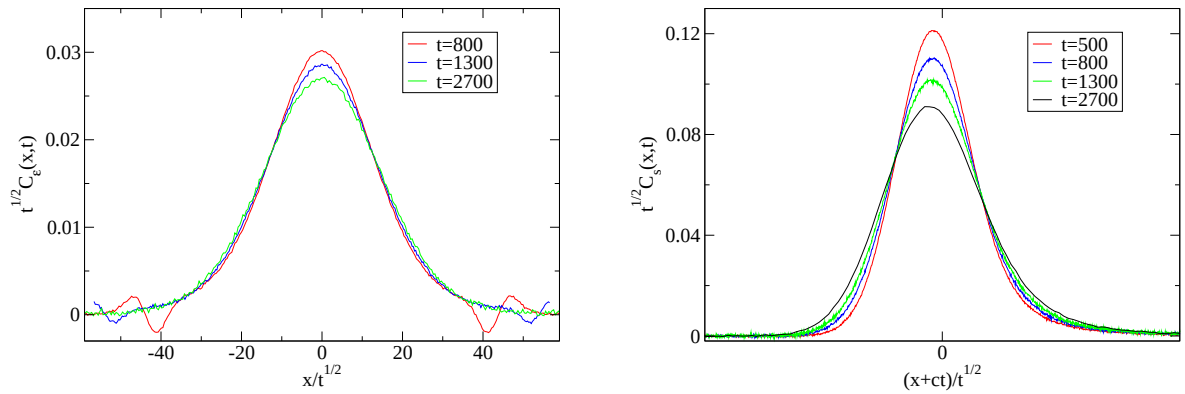

Figure 3.3: Set I: Scaled plots of heat mode and right moving sound mode correlations, at different times, using a diffusive scaling ansatz. The parameters in the simulation were $k_2 = 1, k_3 = 2, k_4 = 1, T = 0.5, P = 1.0$ and $N = 8192$. We see here that the collapse of different time data is very good. The fit o the Levy-stable distribution with $\lambda_e = 13.8$ is quite good while the fit to the KPZ scaling function is not so good.

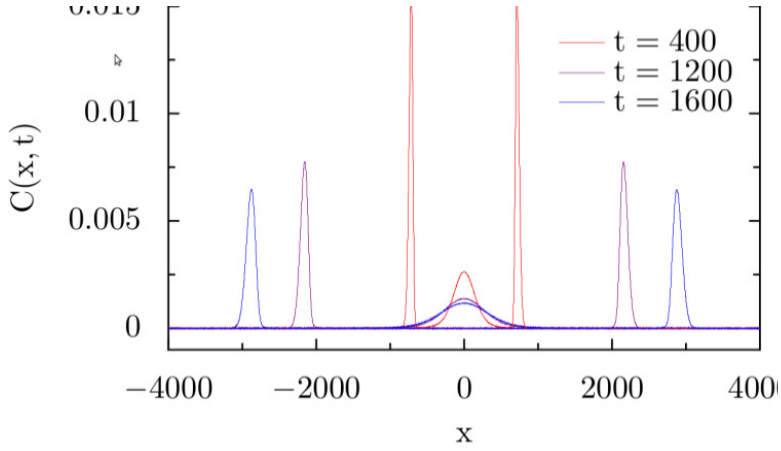

FIGURE 3.4: Set II: Heat and sound mode correlations at three different times for the parameter set as in Fig. (3.1) but with $T = 5.0$. The speed of sound in this case was $c = 1.80293$ and the system size was $N = 8192$. In this case we see that the separation of the heat and sound modes is faster and more pronounced than for the parameter set of Fig. (3.1).

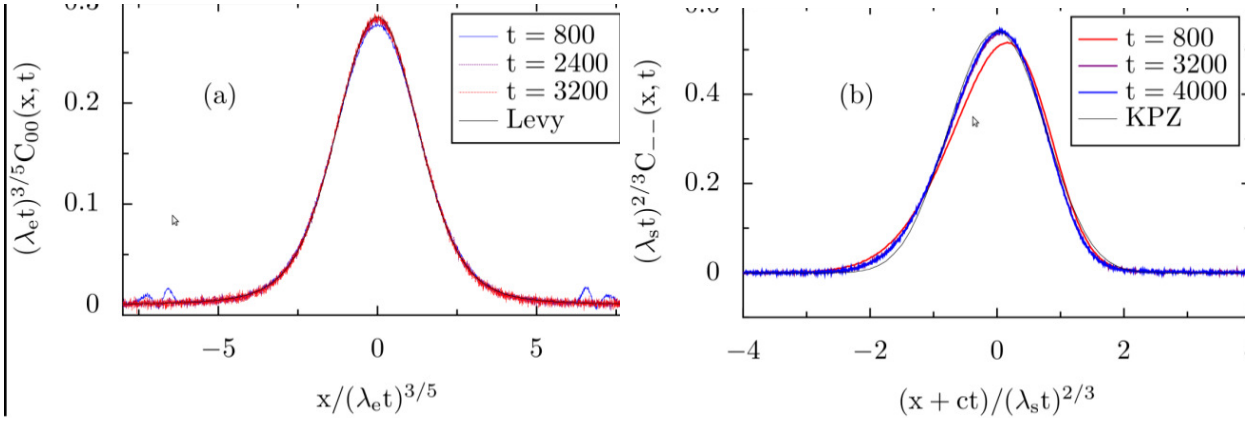

FIGURE 3.5: Set II: Scaled plots of heat mode and left moving sound mode correlations at different times, using a Levy-type-scaling for the heat mode and KPZ-type scaling for the sound mode. The parameters in the simulation were $k_2 = 1, k_3 = 2, k_4 = 1, T = 5.0, P = 1.0$ and $N = 8192$. We see here that the collapse of different time data is very good. Again we find a very good fit to the Levy-stable distribution with $\lambda_e = 5.86$ while the fit to the KPZ scaling function is poor.

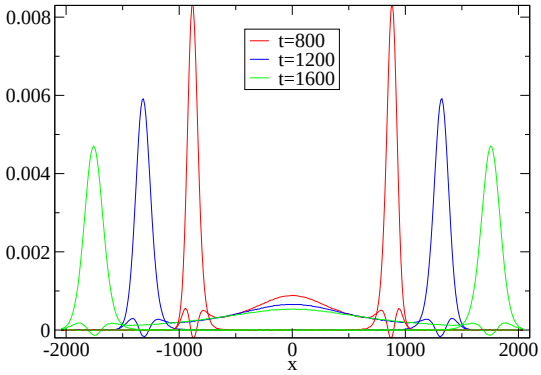

Figure 3.6: Set III: In this plot we show the heat mode correlation and the two sound mode correlations at three different times. At the latest time we see that the heat and sound modes are well separated. The parameters of the Hamiltonian are $k_2 = 1,\ k_3 = -1,\ k_4 = 1,\ T = 0.1,\ P = 0.07776$ and $N = 4096$.

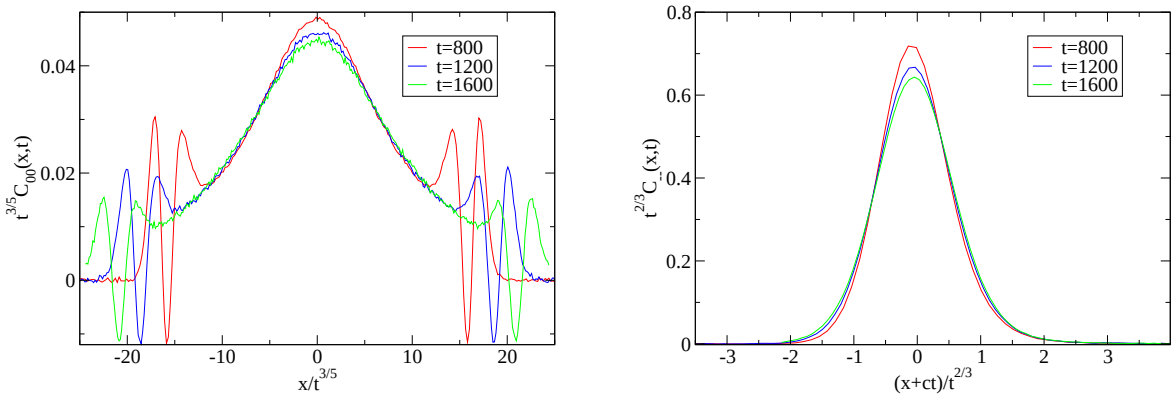

Figure 3.7: Set III: Scaled plots of heat mode and left moving sound mode correlations, at different times, using a Levy-type-scaling for the heat mode and KPZ-type scaling for the sound mode. The parameters in the simulation were $k_2 = 1, k_3 = -1, k_4 = 1, T = 0.1, P = 0.07776$ and $N = 4096$. We see here that the collapse of different time data for the heat mode is reasonably good.

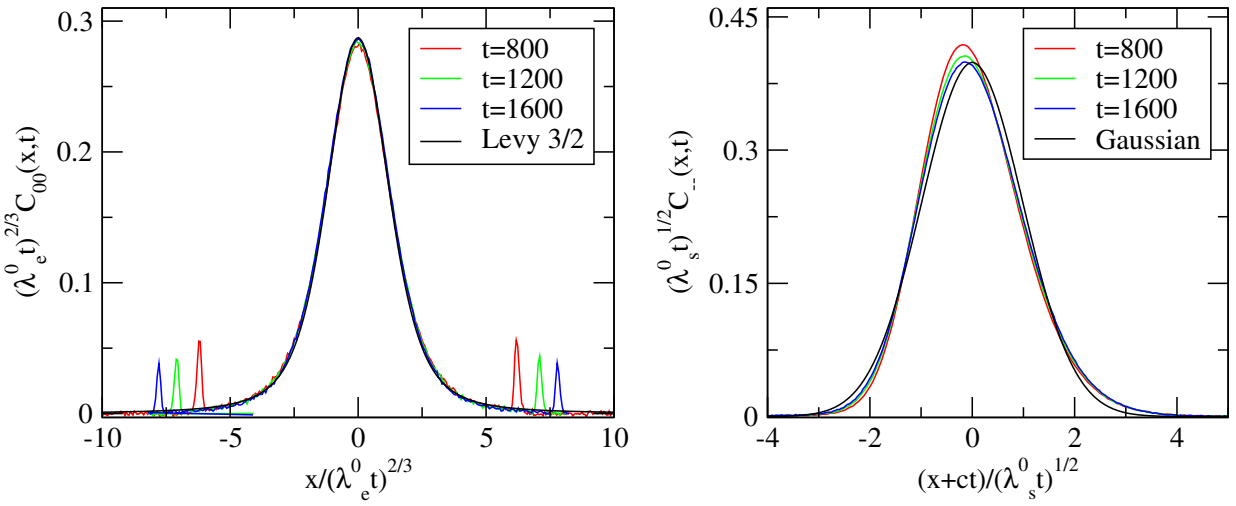

FIGURE 3.8: Set IV: The parameters of the Hamiltonian are $k_2 = 1, k_3 = 0, k_4 = 1$, $P = 0$, $T = 1$ and $N = 8192$. The scaling used here corresponds to Eq. (3.7,3.8), with $\lambda^0_s = .416$ and $\lambda^0_e = 3.18$.

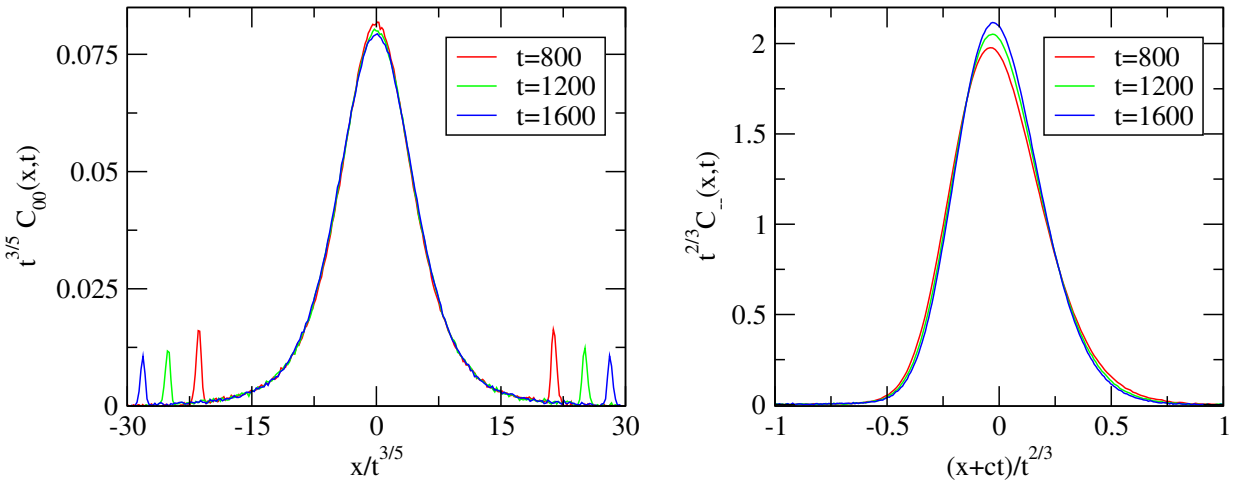

FIGURE 3.9: Set IV: The parameters of the Hamiltonian are $k_2 = 1, k_3 = 0, k_4 = 1$, $P = 0$, $T = 1$ and $N = 8192$. The scaling used here corresponds to Eq. (3.5,3.6). We see that the scaling is not as good as in Fig. (3.8).

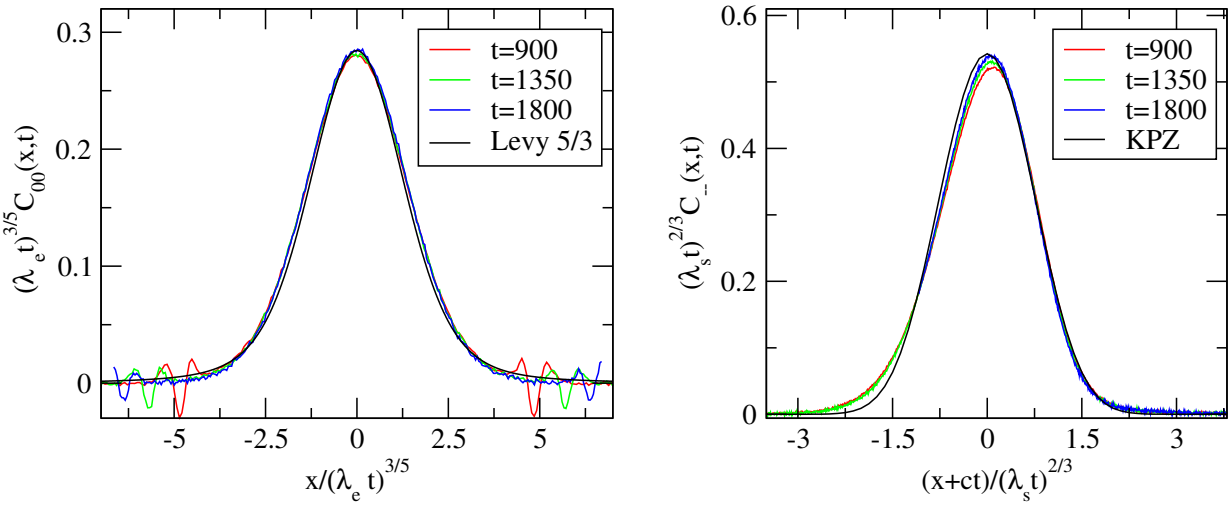

FIGURE 3.10: Set V: The parameters of the Hamiltonian are $k_2 = 1, k_3 = 0, k_4 = 1$, $P = 1$, $T = 1$ and $N = 3200$. The scaling used is the same as for Sets I and II.

However the sound-mode scaling function still shows significant asymmetry and is different from the KPZ function. The theoretical obtained values of $\lambda_s = 0.396$ and $\lambda_e = 5.89$ are now close to the numerically estimated values $\lambda_s = 0.46$ and $\lambda_e = 5.86$.

Set III: $k_2 = 1.0, k_3 = -1.0, k_4 = 1.0, T = 0.1, P = 0.07776$. Our third choice of the parameter set is motivated by recent nonequilibrium simulations [8, 9] which find that the thermal conductivity κ at low temperatures seems to converge to a size-independent value, as discussed in the previous chapter. We suggested that this could be a finite size effect [32]. Here we want to check if the heat mode correlations show any signatures of diffusive heat transport and if they provide any additional insight regarding the strong finite size effects seen in the nonequilibrium studies. The temperature chosen is $T = 0.1$, which for the FPU potential parameters above correspond to the regime at which normal conduction has been proposed.

The speed of sound is calculated to be $c = 1.09352$, which matches with the numerical data, as seen in Fig. (3.7). The heat mode seems to follow the predicted anomalous scaling reasonably well (though the convergence is, as expected, slower than in the high-temperature case). We have checked that the same data, when scaled as $t^{1/2} C_{00}(x/t^{1/2})$ for different times, shows no indication of convergence. Thus we find no evidence for normal heat diffusion at low temperatures. The sound mode agrees quite well with the KPZ-type scaling exponents observed for higher temperatures, though the shape of the correlation function remains asymmetric as in

the high-temperature case. It will be noted that the heat mode shows two peaks near the edges which do not follow the Lévy scaling - these peaks arise from interaction with the sound modes, indicating that there is still some overlap between the two modes near the edges. The sound mode, on the other hand, is found to be undistorted, which is consistent with the prediction from [7] that at long times the mode-coupling equations for the sound modes becomes independent of the heat mode, but not vice versa. The same effect can be seen in sets I and II, but are less pronounced as the modes separate more quickly at higher temperatures.

Set IV: $k_2 = 1.0, k_3 = 0.0, k_4 = 1.0, T = 1.0, P = 0.0$. This is the special case of an even potential at zero pressure for which the prediction from the hydrodynamic theory is a diffusive sound mode, while the heat mode is Lévy but with a different exponent. The predicted scalings are given in Eqs. (3.7,3.8). The speed of sound for this case is $c = 1.46189$. We see from Fig. (3.8) that the proposed scaling leads to an excellent collapse of the heat mode at different times. The sound mode, with diffusive scaling, shows a strong convergence but not yet a collapse. Fig. 3.9 shows the same data but scaled according to the predictions in the non-zero pressure case. It is clear that the data are non-convergent with this scaling. The sound mode is predicted by the theory to be Gaussian, Eq. (3.7), but as seen from Fig. (3.8), the fit to the Gaussian form is poor. From the data we estimate that $\lambda_s^0 = 0.416$, and upon using Eq. (3.10), we find $\lambda_e^0 = 1.17$, whereas the numerically obtained value is 3.18. **Set V**: $k_2 = 1.0, k_3 = 0.0, k_4 = 1.0, T = 1.0, P = 1.0$ Parameters are identical to the above set, except that the pressure is non-zero. Since the potential is even, the pressure arises from externally applied stress to the system. The speed of sound is $c = 1.59143$. We find in Fig. 3.10 that the correlations satisfy the same scaling as for asymmetric potentials with non-zero pressure (as in sets I, II, III). This confirms that the universality class is determined by the asymmetry of $V(r) + Pr$ and not of $V(r)$ by itself.

3.4 Conclusions

For the FPU chain at non-zero pressure, we find that the heat mode scales according to the Levy-$5/3$ distribution, as predicted by fluctuating hydrodynamics, both at high and low temperatures. This implies that in one-dimensional heat transport (in momentum-conserving systems)

the scaling is universally anomalous, and the hypothesis of a non-equilibrium phase transition from normal to anomalous conduction probably does not hold. For the zero-pressure case, the heat mode scales according to the Levy-3/2 distribution as predicted, thus confirming the existence of a second universality class for heat transport in one-dimensional momentum-conserving systems.

For non-zero pressure the sound mode inspirationally scales with the same exponents as the KPZ function, but the shape of the modes is observed not to have collapsed to the KPZ function. This could be because the simulation times are not in the asymptotic regime for the sound modes, which would be consistent with the slowly-decaying correction terms to the scaling forms of the sound mode as discussed in [7]. Thus the prediction that the the sound mode correlations have the form of the KPZ function is not conclusively verified.

The case of zero pressure is very similar, with the sound mode satisfying diffusive scaling, but the limit of the Gaussian scaling form is not reached in our simulations.

Although the Levy stable distribution fits the heat modes very well, we find that at low temperatures the theoretically predicted values for the scaling coefficients λ_s and λ_e do not match the numerical values well. This is consistent with the numerical study in [16], where the authors find that for certain hard-point potentials the scaling forms show an excellent match, but the scaling coefficients are still drifting and one might expect them to converge to the predicted values at larger times. However at high temperatures where the modes are well-separated, the theoretical λ_e matches very well with the numerical data, and the theoretical λ_s is not far off from the numerically obtained value.

The studies here confirm that heat conduction in one- dimensional chains is anomalous and is universal, except for the special case of zero pressure and even potentials. Thus the heat conduction exponent is $\alpha = 1/3$ for the general case of non-zero pressure, and $\alpha = 1/2$ for the special case of zero pressure (see [7] for details).

But notice that neither of this were confirmed conclusively through the steady-state simulations in Chapter 2. It remains an an open and important problem to tie up the picture obtained from the correlation dynamics in our equilibrium studies, with simulations of the steady state in Chapter 2 and the various related results cited there. In the momentum-conserving anharmonic systems that apparently show normal transport, the nonequilibrium simulations indicate an apparent saturation of the thermal conductivity with increasing system size, while equilibrium

studies show an integrable decay of current autocorrelations, as discussed before. Some of our simulations in this chapter were in fact done in parameter regimes (low temperatures, asymmetric potentials) where diffusive-like transport had been reported in earlier work based on nonequilibrium simulations. However, we do not see any signatures of this apparent diffusive behavior, even at intermediate times. This discrepancy is possibly related to finite-size effects coming from the boundaries, which are not present in the equilibrium studies with periodic boundary conditions. This conclusion is further supported by the quantitative differences seen between the free and fixed boundary conditions in the previous chapter. However, more thorough studies are required for a convincing resolution of the problem of finite-size effects.

APPENDIX

The matrix R, which diagonalizes the matrix A, is given by

$$R = \sqrt{\frac{2\beta}{c^2}} \begin{pmatrix} \partial_l p & -c & \partial_e p \\ \widetilde{\kappa} p & 0 & \widetilde{\kappa} \\ \partial_l p & c & \partial_e p \end{pmatrix}, \tag{3.13}$$

where the columns, including the normalization factor, provide the right eigenvectors V_α, $\alpha = -1, 0, 1$, of the A matrix. The Hessian tensor H encodes the quadratic corrections to the couplings between the original hydrodynamic variables. $H^\alpha_{\beta\gamma}$ represents the coupling of the field component α to the field components β, γ. The tensor can be represented through three 3×3 matrices, one for each value of α,

$$H^r = 0, \;\; H^u = \begin{pmatrix} \partial_l^2 p & 0 & \partial_l \partial_e p \\ 0 & -\partial_e p & 0 \\ \partial_l \partial_e p & 0 & \partial_e^2 p \end{pmatrix}, \;\; H^e = \begin{pmatrix} 0 & \partial_l p & 0 \\ \partial_l p & 0 & \partial_e p \\ 0 & \partial_e p & 0 \end{pmatrix}.$$

After transforming to the normal modes $\vec{\phi}$, the nonlinear hydrodynamic equations become

$$\partial_t \phi_\alpha = -\partial_x \left[c_\alpha \phi_\alpha + \langle \vec{\phi}.G^\alpha \vec{\phi} \rangle - \partial_x (D\phi)_\alpha + (B\xi)_\alpha \right] .$$

The term in angular brackets is the inner product of G^α with respect to $\vec{\phi}$. Also, $D = R\widetilde{D}R^{-1}$ and $B = R\widetilde{B}$ satisfy the fluctuation-dissipation relation $BB^T = 2D$. The vector $\vec{c} = (-c, 0, c)$. The tensor G represents the coupling between the normal modes and is given by

$$G^\alpha = \frac{1}{2} \sum_{\alpha'=-,0,+} R_{\alpha\alpha'} (R^{-1})^T H^{\alpha'} R^{-1}. \tag{3.14}$$

The elements of G^α can be represented through cumulants of V, r with respect to the single site distribution up to order three, see [**?**].

The values of R and G^0 and G^1 are given below. The elements of G^{-1} are a rearrangement of the elements of G^1 as follows from $G^{-1}_{-\alpha\ -\beta} = -G^1_{\alpha\beta}$, $G^{-1}_{-10} = G^{-1}_{01}$ and $G^{-1}_{\alpha\beta} = G^1_{\beta\alpha}$ [**?**]. The long time behavior is dominated by the diagonal G entries. The off-diagonal entries are irrelevant. G^s_{ss} are the self-couplings. Note that $G^0_{00} = 0$, as claimed before. Also for the even potential at zero pressure case the only leading terms are G^0_{ss}, $s = \pm 1$. There is considerable variation in the diagonal matrix elements.

Set I

$$R = \begin{pmatrix} -0.7935 & -1. & 0.66118 \\ 1.89594 & 0.0 & 1.89594 \\ -0.7935 & 1. & 0.66118 \end{pmatrix}, \quad G^0 = \begin{pmatrix} -0.689497 & 0.0 & 0.0 \\ 0.0 & 0.0 & 0.0 \\ 0.0 & 0.0 & 0.689497 \end{pmatrix},$$

$$G^1 = \begin{pmatrix} -0.24236 & -0.075565 & .238543 \\ -0.075565 & -0.0669417 & -0.075565 \\ .238543 & -0.075565 & 0.238543 \end{pmatrix}.$$

Set II

$$R = \begin{pmatrix} -0.547157 & -0.316228 & 0.0229798 \\ 0.229483 & 0.0 & 0.229483 \\ -0.547157 & 0.316228 & 0.0229798 \end{pmatrix}, \quad G^0 = \begin{pmatrix} -1.03436 & 0.0 & 0.0 \\ 0.0 & 0.0 & 0.0 \\ 0.0 & 0.0 & 1.03436 \end{pmatrix},$$

$$G^1 = \begin{pmatrix} -.0671336 & .240399 & .140022 \\ .240399 & -.152971 & .240399 \\ .140022 & .240399 & .140022 \end{pmatrix}.$$

Set III

$$R = \begin{pmatrix} -2.3376 & -2.23607 & 1.38344 \\ 0.793106 & 0.0 & 10.1994; \\ -2.3376 & 2.23607 & 1.38344 \end{pmatrix}, \quad G^0 = \begin{pmatrix} -0.55766 & 0.0 & 0.0 \\ 0.0 & 0.0 & 0.0 \\ 0.0 & 0.0 & 0.55766 \end{pmatrix},$$

$$G^1 = \begin{pmatrix} -0.0721968 & 0.0206018 & 0.0790847 \\ 0.0206018 & -0.0353259 & 0.0206018 \\ 0.0790847 & 0.0206018 & 0.0790847 \end{pmatrix}.$$

Set IV

$$R = \begin{pmatrix} -1.03371 & -0.707107 & 0.0 \\ 0.0 & 0.0 & 1.09893 \\ -1.03371 & 0.707107 & 0.0 \end{pmatrix}, \quad G^0 = \begin{pmatrix} -0.803254 & 0.0 & 0.0 \\ 0.0 & 0.0 & 0.0 \\ 0.0 & 0.0 & 0.803254 \end{pmatrix},$$

$$G^1 = \begin{pmatrix} 0.0 & 0.133622 & 0.0 \\ 0.133622 & 0.0 & .133622 \\ 0.0 & .133622 & 0.0 \end{pmatrix}.$$

Set V

$$R = \begin{pmatrix} -0.964170 & -0.707106 & -0.964171 \\ 1.05385 & 0.0 & 1.05385584 \\ 0.161141 & 0.707107 & 0.161141 \end{pmatrix}, \quad G^0 = \begin{pmatrix} -0.838569 & 0.0 & 0.0 \\ 0.0 & 0.0 & 0.0 \\ 0 & 0 & 0.838569 \end{pmatrix},$$

$$G^1 = \begin{pmatrix} -0.112782 & 0.07359 & 0.143663 \\ 0.07359 & -0.104607 & 0.07359 \\ 0.143663 & 0.07359 & 0.143663 \end{pmatrix}.$$

4

Normal Heat Transport in the Coupled Rotator Model: Role of Conserved Quantities

4.1 Introduction

The previous two chapters show that heat transport in anharmonic chains is quite generically anomalous. While some doubts remain regarding the precise value of the exponents and the form of the sound-mode correlation functions, that conduction in the Fermi-Pasta-Ulam model is anomalous, at least in the high-temperature regime, seems to be evident. Further, if nonlinear fluctuating hydrodynamics is to be believed, the exponents hold for all non-integrable models with three conserved quantities and at all temperature regimes. This brings us back to one of the

central questions of the thesis: Is there a one-dimensional translationally invariant model where heat transport is normal?

Assuming that the fluctuating hydrodynamic theory is correct, a third universality class could exist only for systems which have less than three conserved quantities. Interestingly, a simple model in that class has already been numerically studied in the literature, namely the model of coupled rotators on a one-dimensional lattice, but it has so far not been realized that the model has only two conserved fields, and therefore its hydrodynamics should be distinct from generic anharmonic chains, such as the much-studied Fermi-Pasta-Ulam model. In this chapter we show that stretch is not a conserved field in the coupled-rotator model, and this leads to a linear two-variable hydrodynamics, where on a sufficiently coarse-grained scale the currents are represented solely by noise and dissipation terms. This straightforwardly leads to a Gaussian solution for the spread of momentum and energy packets. As an outcome of our analysis, we propose some general criteria for normal transport based on the existence of conservation laws.

Section 4.2 discusses the implications of fluctuating hydrodynamics for anomalous transport in one dimension. Section 4.3 identifies the coupled rotator model as constituting an exception to the usual hydrodynamic treatment of momentum-conserving models. Numerical and analytical results demonstrating normal transport of momentum and energy are presented, and the low-temperature regime is discussed. Section 4.4 presents a unified picture of the hydrodynamic criteria for normal transport of conserved quantities in one dimension.

4.2 Fluctuating hydrodynamics and anomalous transport

We briefly recapitulate the basic ideas behind fluctuating hydrodynamics. Consider one-dimensional systems on a ring, each particle described by a coordinate $q(x)$ and momentum $p(x)$, with $x = 1, \ldots, N$. Defining $r(x) = q(x+1) - q(x)$, the Hamiltonian is written as $H = \sum_{x=1}^{N} e(x)$, where $e(x) = \frac{p^2(x)}{2} + V[r(x)]$. The key ingredient in hydrodynamics is to identify the locally conserved fields in the system, with their fluctuations around the equilibrium value represented by the vector $\vec{u}(x,t) = \{u_1, \ldots, u_n\}$ for n conserved variables. The corresponding currents are denoted by $\vec{j}(x,t)$. In fluctuating hydrodynamics, as we saw earlier, one adds noise and dissipation

terms to the currents, and takes the continuum limit to obtain

$$\partial_t u_\alpha = -\partial_x \left[j_\alpha - \partial_x D_{\alpha\beta} u_\beta + B_{\alpha\beta}\xi_\beta \right] \ , \tag{4.1}$$

where the noise terms ξ are stationary Gaussian processes satisfying $\langle \xi_\alpha(x,t) \rangle = 0$ and $\langle \xi_\alpha(x,t)\xi_\beta(x',t') \rangle = \delta_{\alpha\beta}\delta(x-x')\delta(t-t')$. The noise and dissipation matrices B, D, satisfy the fluctuation-dissipation relation $DC^0 + C^0 D = BB^T$, where $C^0_{\alpha\beta}(x) = \langle u_\alpha(x,0)u_\beta(0,0) \rangle$, angular brackets denoting equilibrium averages.

It is important to understand what the stochastic and dissipative terms physically represent. In deriving the continuum hydrodynamic equations, one necessarily loses information about the short-wavelength behavior, with the continuum equations containing only the modes that relax on the longest length and time scales. Although a rigorous derivation is lacking, the fluctuation and dissipation terms may be taken to represent the effects of the faster modes on the long-wavelength behavior of the system. The fluctuation-dissipation relation asserts that these modes are thermalized, whereas the lack of correlation of the noise terms in space and time indicate their fast relaxation in equilibrium. It should also be possible in principle to derive the diffusion coefficients in Eq. (4.1) following the Hamiltonian derivation of the Navier-Stokes equations in [33].

In a general one-dimensional non-integrable system, such as the FPU lattice described in Chapter 3, one has three conserved fields and corresponding currents given respectively by $\vec{u} = (r, p, e)$ and $\vec{j} = (-p, P, pP))$, where the field now represents the local fluctuations of stretch, momentum and energy about their respective equilibrium values. The local pressure field is $P(x,t) \equiv -\partial_r V(r(x,t))$, and the thermodynamic pressure is given by $\bar{P} = -\langle \partial_r V(r) \rangle$. This is the case addressed in [7] (see Chapter 3) where the hydrodynamics is treated by expanding the currents up to second order in the fields:

$$j_\alpha = A_{\alpha\beta}u_\beta + H^\alpha_{\beta\gamma}u_\beta u_\gamma \ . \tag{4.2}$$

The tensors A and H are expressed in terms of the derivatives of the pressure $\bar{P}$ with respect to the energy and volume of the corresponding microcanonical ensemble, using Maxwell-type thermodynamic relations. When the expansion is truncated to first order (i.e set $H^\alpha_{\beta\gamma} = 0$), the resulting linear hydrodynamics can be diagonalized to obtain the three normal modes ϕ_α. The

second-order terms in the expansion can then be expressed as a coupling between these normal modes ϕ_α, as we saw earlier, and the dynamical correlators $\langle\phi_\alpha(x,t)\phi_\beta(0,0)\rangle$ of the resulting theory are calculated within a mode coupling approximation. In particular one finds that the heat mode correlations exhibit superdiffusive (Levy) scaling, which implies super-diffusive transport of heat and universal non-zero values for a.

To explore the possibility of normal diffusion of heat, one has to look for cases in which there are less than three conserved fields, and hence the hydrodynamics as developed in [7] does not apply. Since energy is necessarily a constant of motion, the only possibilities are where either the stretch $r(x)$ or the momentum $p(x)$ (or both) are not conserved. We claim that any of these cases lead to normal transport of energy. The case of non-conservation of momentum has been treated quite extensively through several models in the literature, and thus we focus primarily on the case where stretch is not conserved. However, as we shall see later, the hydrodynamics of the energy mode is practically identical for the two cases.

4.3 The Coupled Rotator model

To explore the case of non-conserved stretch, consider a Hamiltonian H with $V(r) = V_0\cos(r)$, commonly known as the coupled rotator (CR) model. Convincing numerical evidence [34, 35] exists for a finite thermodynamic conductivity in this model, based on direct molecular dynamics simulations of the steady state as well as equilibrium current autocorrelations. Note that since the potential is periodic, the angle variables $r(x)$ should be taken to lie within an appropriate finite range to ensure that the partition function is finite and therefore the canonical ensemble is well-defined. For our analysis we restrict it within the interval $(0, 2\pi)$, although any range that is an integer multiple of 2π should be expected to have identical macroscopic properties. The equation of motion of $r(x)$ within the range $(0, 2\pi)$ is $\dot{r}(x) = p(x+1) - p(x)$, but since r is restricted within the cell, one should add boundary terms at 0 and 2π such that the $r(x)$ are reset whenever the prescribed range is exceeded. This discontinuity in $r(x)$ is not in general compensated by a simultaneous change in the nearest neighbors, which means that $r(x)$ is not a locally (or globally) conserved field.

This crucial observation implies that the thermodynamic conjugate of stretch, the pressure $\bar{P}$,

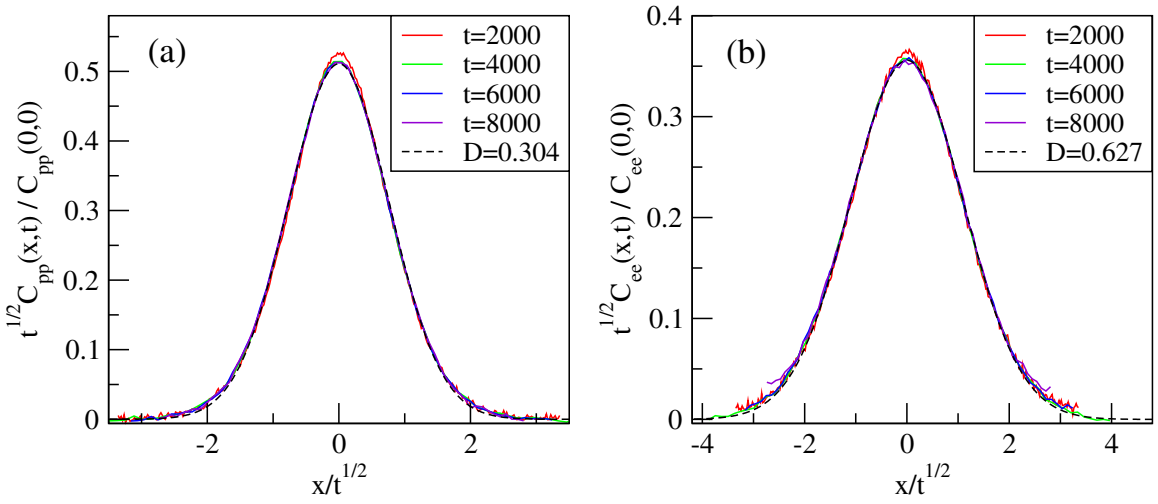

Figure 4.1: Plot of the autocorrelation of momentum (left) and energy (right), scaled in accordance with normal diffusion and normalized with $C(0,0)$, which is computed numerically from the equilibrium distribution. The dashed black lines correspond to normalized Gaussians with the respective diffusion constants mentioned in the figures.

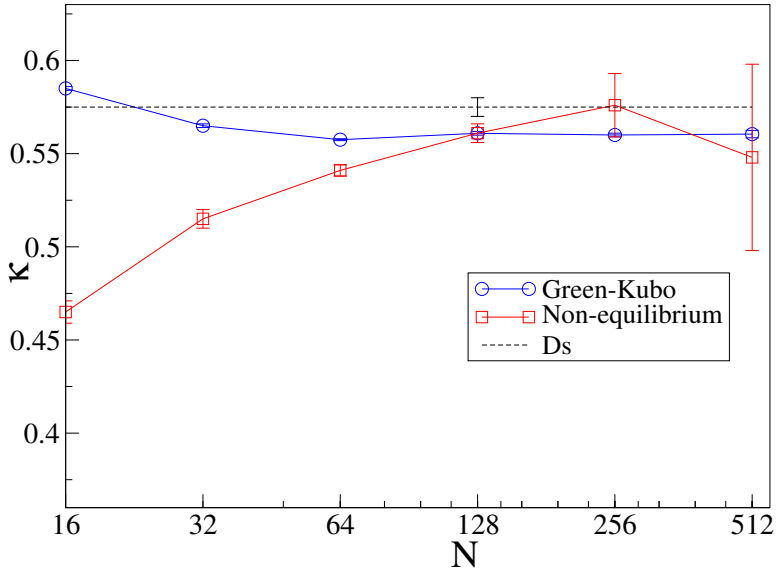

Figure 4.2: Plot of conductivity through three different methods. The circles and the boxes show the size-dependent behavior of the conductivity as obtained from the Green-Kubo formula and direct nonequilibrium simulations respectively. The dashed straight line is the value of the conductivity as predicted from the specific heat density and the diffusivity of the heat mode.

is necessarily zero. In the case of stretch-conserving models, a non-zero pressure is incorporated into the equilibrium description by modifying the Gibbs weight of each microstate such that $Prob(\{r(x)\}) \sim \Pi_x \; e^{-\beta[V(r(x))+\bar{P}r(x)]}$. This measure remains invariant under the dynamics since $\sum_x r(x)$ is conserved. However, when the stretch is not conserved, as in the case of the CR model, the measure is invariant only for $\bar{P} = 0$. It is important to emphasize that the equilibrium pressure of the rotator model is *identically* zero, unlike the special case of zero pressure in stretch conserving systems, where the derivatives of pressure with respect to energy and volume are finite even at zero pressure and thus the normal modes remain coupled [7]. For the CR model, the non-conserved field r drops out from the hydrodynamic description. Since $\bar{P}$ is identically zero, the coupling tensors A and H in Eq. (5.4) (and any higher-order terms that may be included) vanish, and the hydrodynamic currents j are zero. The local pressure continues to fluctuate on a microscopic scale, but these fluctuations are effectively incorporated into the noise and dissipation terms in the net current. Thus the conserved field in this model is $\vec{u} = (p, e)$, and the corresponding hydrodynamic equations are

$$\partial_t u_\alpha = -\partial_x \left[-\partial_x D_{\alpha\beta} u_\beta + B_{\alpha\beta}\xi_\beta \right] \; . \tag{4.3}$$

As in the case of stretch-conserving systems, we find numerically that the cross-correlations decay rapidly, and then the auto-correlations $C_{\alpha\alpha}(x,t) \equiv \langle u_\alpha(0,0) u_\alpha(x,t) \rangle$ can be shown to be

$$C_{\alpha\alpha}(x,t) = \frac{1}{\sqrt{4\pi D_{\alpha\alpha} t}} \exp \left[-\frac{x^2}{4 D_{\alpha\alpha} t} \right] \; , \tag{4.4}$$

implying diffusive transport of both momentum and energy. Sound modes are absent in the hydrodynamic limit.

We check these predictions with numerical simulations. We have performed molecular dynamics simulations of the CR model in equilibrium, choosing the initial conditions from the Gibbs distribution, and integrating the system using the fourth order Runge-Kutta as well as the velocity Verlet algorithm. The normalized correlation functions of momentum, $C_{pp}(x,t)/C_{pp}(0,0)$ and energy, $C_{ee}(x,t)/C_{ee}(0,0)$ are shown in Fig. (4.1), for $V_0 = 1$ temperature $T = 1$ and a system of size $N = 400$. The momentum and energy modes have been scaled diffusively and show excellent collapse. In fact, the scaled correlation functions are fitted very well by Gaussian functions (dashed curves), showing that the correlation functions are as predicted in Eq. (4.4). Note that

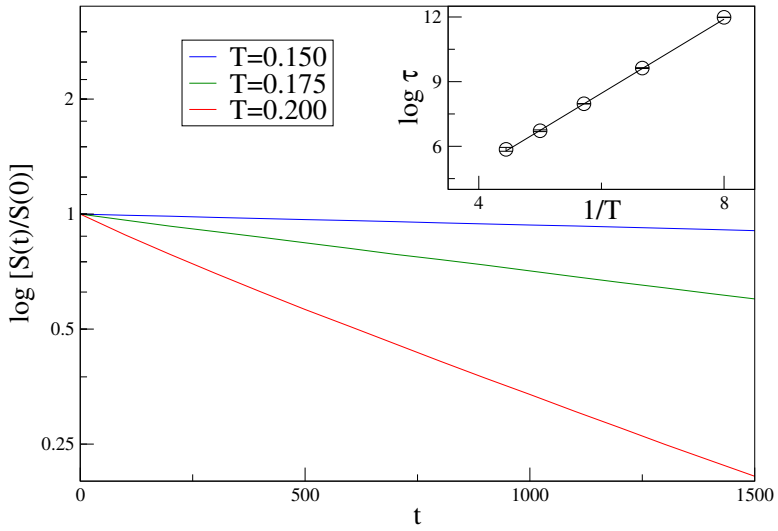

Figure 4.3: Plot of $S(t)$ at various temperatures for the CR model with $V_0 = 1$. Note that the decay is exponential, and even at the lowest temperature a slow decay is evident. The inset shows the logarithm of the correlation time against $1/T$, which appears linear. The straight line fit is $y = 1.72x - 1.86$, so that $\Delta E = 1.82$, which is in reasonable agreement with the expected value 2 at this level of approximation.

the form of these correlation functions are completely different from the ones in systems with three conserved fields, where one finds a non-Gaussian central peak in addition to traveling sound peaks. We must mention that similar diffusive nature of momentum correlations in the rotator model have recently been reported in [36].

Using Fourier's law it can be shown that $\kappa = Ds$, where D is the energy diffusivity and s is the specific heat density. For the present system with $V_0 = 1$ it is calculated that the partition function $Z = \int_{-\infty}^{\infty} dp\ e^{-\frac{1}{2}\beta p^2} \int_0^{2\pi} dr\ e^{-\beta\cos(r)} = \sqrt{\frac{2\pi}{\beta}} I_0(\beta)$, where $I_n(x)$ is the n-th modified Bessel function of the first kind. From this one finds that

$$s \equiv \frac{1}{T^2}\frac{\partial^2}{\partial\beta^2} lnZ = \frac{1}{2}\left[1 + \beta^2(1 + \frac{I_2(\beta)I_0(\beta) - 2I_1(\beta)^2}{I_0(\beta)^2})\right].$$

For our parameters, $s = 0.9168$, and using D as determined from the numerical fitting in Fig. (1b), we get $\kappa = 0.5749$.

We compare this value with the conductivity obtained directly through two other independent ways. When the conductivity is finite, then from the Green-Kubo formula it is given by

$$\kappa = \lim_{\tau\to\infty} \frac{\langle Q_\tau^2\rangle}{2NT^2\tau},$$

where $Q_\tau = \int_0^\tau J(t)dt$, and the total heat current $J = \sum_{x=1}^{N} p(x)\partial V/\partial r(x)$. The average is

over the equilibrium ensemble at temperature T. A second way of determining κ is through direct non-equilibrium simulation of the heat current. Two ends of the rotor chain are connected to Langevin baths at temperatures $T \pm \Delta T$, and the resulting steady-state heat current is calculated and the conductivity is obtained from the standard definition. In both these cases, κ is computed from simulations performed for different of system sizes. In Fig. 4.2, we see that the conductivity from the Green-Kubo formula converges to the value $\kappa \approx 0.56$, in close agreement with the value predicted from the diffusivity above. The values from the non-equilibrium simulations are similar, but the larger error bars make a precise comparison difficult.

To understand the non-conservation of stretch more clearly, we notice that for any conserved field u with zero mean, the following exact sum rule holds:

$$\sum_x \langle u(0,0)u(x,t)\rangle = \sum_x \langle u(0,0)u(x,0)\rangle = \langle u^2(0,0)\rangle,$$

where the last equality is for initial conditions with a product measure. Since $r(x)$ is not conserved in the CR model, we expect $S(t) \equiv \sum_x \langle r(0,0)r(x,t)\rangle$ to decay with time and go to zero at long times. Since the non-conservation is a consequence of periodicity, the time-scale associated with the decay of $S(t)$ must be the time-scale required for the variables r_i to reach the boundary of the interval $[0, 2\pi]$, or equivalently for the time required for the particle to escape the potential well represented by one wavelength of the potential. In the limit of low temperature, this time-scale approaches the Kramers escape time $\tau \sim \exp(\Delta E/T)$. In other words, at low temperatures we expect $S(t) \sim \exp(-t/\tau)$, with τ proportional to $\exp(2/T)$. Fig. 4.3 shows the exponential behavior of $S(t)$, and the inset shows that the decay time indeed scales with T approximately as predicted (see caption for details). It was reported in [35] that there exists a transition from anomalous to normal diffusion in the CR model between $T = 0.2$ and $T = 0.3$. However, as seen in Fig. 4.3, the $S(t)$ correlation continues to decay at temperature 0.2 and below, but the very slow rate of decay means that it is hard to numerically observe the asymptotically converging thermal conductivity on numerically accessible scales. So the apparent anomalous diffusion reported in [35] is possibly a finite-size effect. Similar objections to the claim was made in [34, 37], though not from the viewpoint of conservation laws.

At low temperatures, each angle variable spends most of its time fluctuating near the potential

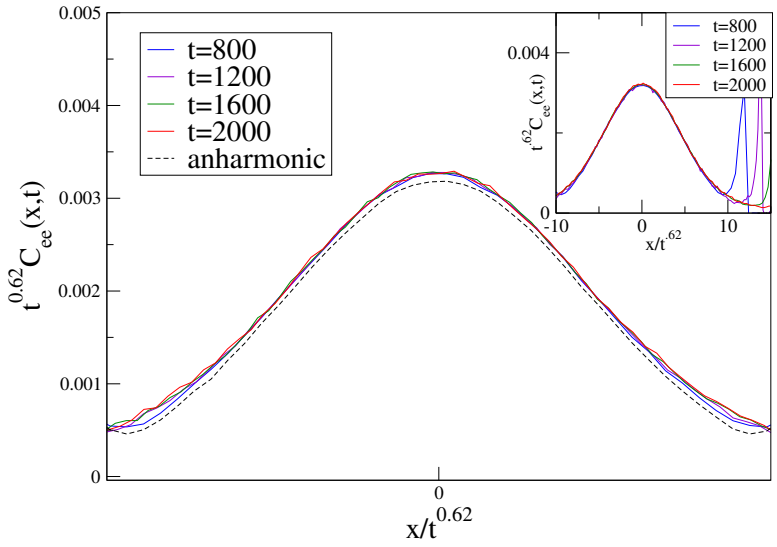

FIGURE 4.4: Scaled plots of $C_{ee}(x)$ for the CR model, for $T = 0.2$. The dashed line is for the corresponding anharmonic model, at $t = 800$. Including higher order terms in the anharmonic potential should produce an even better approximation. The inset shows the corresponding plots for the anharmonic model with the same scaling.

minimum. Thus at short times, the hydrodynamics must be well-approximated by an anharmonic expansion of the CR potential around the minimum at $r = \pi$, while the crossover to normal diffusive behavior should occur at the time-scales indicated in Fig. (4.3). To check this, we consider the anharmonic chain obtained after truncating the CR potential at the first stable anharmonic term, obtaining $V(r) = r^2/2 - r^4/24 + r^6/720$. This system has three conserved modes – extension, momentum and energy. For anharmonic chains at zero pressure, hydrodynamics predicts that the heat mode scales as $x \sim t^{2/3}$ [7]. We simulate the equilibrium correlations for this model for comparison.. The energy mode for the CR model (Fig. 4.4) satisfies an anomalous scaling $x \sim t^{0.62}$. The dashed line gives numerical results from the truncated anharmonic potential, which is in reasonable agreement with the CR model up to the simulation time. The inset shows the same correlations for the anharmonic potential with the same scaling. The scaling exponent 0.62 is close to but not yet identical with the prediction in [7], and is presumably due to the slow separation of heat and sound modes at low temperatures as seen in simulations elsewhere [32].

The results for the sound mode are shown in Fig. 4.5. The anharmonic chain (Fig 4.5a) is seen to satisfy a $t^{1/2}$ scaling as predicted from nonlinear fluctuating hydrodynamics, and at short times a similar scaling is observed for the CR model (not shown). However at longer times, the sound

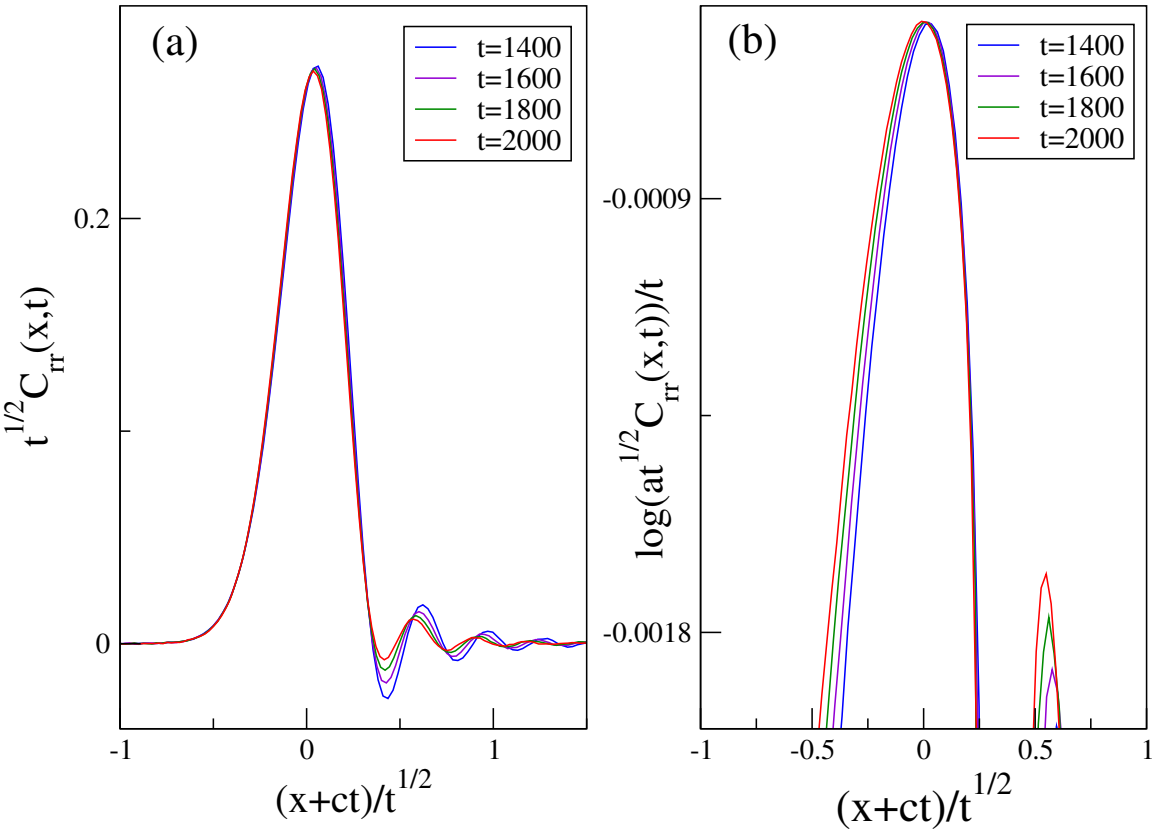

FIGURE 4.5: Plot of $C_{rr}(x,t)$ around the left-moving sound peak for $T = 0.2$. (a) The anharmonic model correlations scaled with $x \sim t^{1/2}$. (b) The CR model scaled similarly with an additional exponentially decaying pre-factor. The sound speed at this temperature is $c = 0.938791$. The constant $a = 3.49$.

peaks of the CR model (Fig. 4.5b) shows a very different behavior. The scaling in the figure indicates that close to the peak the sound mode scales as $C_{rr}(x,t) \sim exp(-t/\tau)\frac{1}{t^{1/2}} f(x/t^{1/2})$, with $\tau \approx 1880$, which is considerably different from $\tau \approx 700$ for $S(t)$ as shown in Fig. 4.3. This is because the scaling form away from the sound peak at these time-scales is not given by $x \sim t^{1/2}$, as is evident from Fig. 4.5b. The exponential term in the sound peak indicates that even at low temperatures the sound modes are transient and disappear on a thermodynamic scale, and one therefore expects the heat mode to show a diffusive scaling at sufficiently long times.

4.4 Conclusions

We realize that an essentially similar scenario occurs in momentum non-conserving models - such as pinned anharmonic chains or the harmonic chain with random velocity flips, with the roles of stretch and momentum fields now interchanged. The hydrodynamic equations for stretch and energy here would be linear with vanishing long-range currents, and both these fields should diffuse normally. The velocity-flip model has already been studied in the hydrodynamic limit quite rigorously, and it has indeed been shown that macroscopic diffusion equations for these fields exist for this model [38].

It has so far been believed that breaking translational symmetry is crucial to normal heat conduction, but the CR model had remained a puzzle. We show that it is not translational invariance but the number of conserved fields that decides whether transport is normal. A generic non-integrable Hamiltonian system has, in addition to energy, at most two conserved quantities - stretch and momentum, and any model that does not conserve either of these exhibits normal diffusion of energy. We believe that our hydrodynamic treatment of the rotator model (which, as should be clear, holds for all one-dimensional systems with periodic inter-particle potentials) establishes this beyond reasonable doubt.

To summarize the central lesson from this chapter, *whenever stretch (momentum) is not conserved in a one-dimensional model, the momentum (stretch) and energy fields exhibit normal diffusion*. The possibility of normal transport in one dimension has been a matter of long-standing debate, and in this work we identify sufficient hydrodynamic criteria for normal transport of energy in one-dimensional systems.

5

Landauer formula for phononic heat conduction in quantum harmonic lattices

5.1 Introduction

We have investigated heat transport in one-dimensional classical systems in detail. The corresponding class of quantum mechanical problems has been treated very rarely in the literature, and a detailed solution of heat transport in nonintegrable quantum systems lies beyond the scope of this thesis. Instead, we focus on a one-dimensional quantum harmonic system and present some exact results.

The heat current across a quantum harmonic system connected to reservoirs at different temperatures is given by the Landauer formula, in terms of an integral over phonon frequencies ω, of the energy transmittance $\mathcal{T}(\omega)$.

The Landauer formula gives an exact expression for the current (energy and/or particle) in non-interacting quantum systems coupled to reservoirs kept at different temperatures (and/or different chemical potentials). The formula for phonon heat current across a harmonic crystal connected to heat baths at temperatures T_L, T_R is given by

$$J = \frac{1}{2\pi}\int_{-\infty}^{\infty} d\omega\ \hbar\omega\ \mathcal{T}(\omega)\ [f(\omega, T_L) - f(\omega, T_R)]\ , \tag{5.1}$$

where the quantity $\mathcal{T}(\omega)$, which we shall refer to as the energy transmittance, can be expressed in terms of appropriate "nonequilibrium" phonon's Green's functions and $f(\omega, T) = 1/(e^{\hbar\omega/k_B T} - 1)$ is the thermal phonon distribution function. This Landauer formula for phononic heat current was proposed in [39] and has been derived rigorously using the quantum Langevin equation approach [11, 40] as well as the nonequilibrium Green's function (NEGF) approach [41, 42]. The energy transmittance $\mathcal{T}(\omega)$ is usually expressed in terms of nonequilibrium phonon Green's function and it is expected that it is related to the transmission coefficient $\tau(\omega)$ of plane waves across the system. In this chapter we demonstrate exact relationships between $\mathcal{T}(\omega)$ and $\tau(\omega)$ for harmonic lattices with arbitrary parameters.

Section 5.2 defines the model and gives the expression for $\mathcal{T}(\omega)$ from NEGF. Section 5.3 finds the scattering state solutions and the transmission coefficients, and relates it to the results of 5.2. Section 5.4 finds the energy current in each mode and gives an exact derivation of the Landauer formula.

5.2 Definition of model and NEGF expression for energy transmittance $\mathcal{T}$

Landauer's original idea was to think of conductance in terms of transmission or scattering of plane waves and for the case where the reservoirs or "leads" are one dimensional, it is expected that $\mathcal{T}(\omega)$ is related to the transmission coefficient $\tau(\omega)$ of plane waves [43]. For the case of electron transmission, $\mathcal{T}(\omega)$ can again be expressed in terms of nonequilibrium Green's functions [44] and the relation to the transmission coefficient was directly demonstrated through the work of Todorov *et* al using scattering theory [45] and also by [46]. For the case of phonons we are not aware of an explicit proof of this relation and that is the main objective of this chapter [47].

Here we consider a general one-dimensional finite harmonic chain coupled to reservoirs which are themselves semi-infinite ordered harmonic chains and give a fully quantum-mechanical derivation of the relation between $\mathcal{T}$ and τ and show how the NEGF current formula can be obtained from the transmission coefficient.

In our derivation we first note that in the NEGF approach the energy transmission $\mathcal{T}$ is expressed in terms of a Green's function. This Green's function can be expressed explicitly in terms of a product of 2×2 matrices. On the other hand the transmission coefficient can be computed by constructing appropriate scattering states and this can be done in two ways — (i) a direct solution of the discrete wave equation which again gives τ expressed in the form of a product of matrices or (ii) by using the Lippmann-Schwinger scattering theory to evolve reservoir normal modes and this gives τ directly in terms of the Green's function. From the forms of these expressions we directly obtain the required relations. We note that for the case where the reservoirs are not one-dimensional chains, but have arbitrary geometries [48–50], the NEGF expression for $\mathcal{T}(\omega)$ still has the same form but it is not clear as to how one should compute τ and how exactly it is related to $\mathcal{T}$. In this case the approach using Lippmann-Schwinger scattering theory can still be used to arrive at the required relation. A model similar to ours was studied recently by Zhang *et* al [51] in the context of interfacial thermal transport in atomic junctions and the relation between the NEGF formula for energy transmittance and the transmission coefficient was established numerically and also exactly for the special case of a single interface.

The plan of this chapter is as follows. In sec. 5.2 we first define the model and state some general results for the heat current given by the formalism of nonequilibrium Green's functions. We then give an explicit expression for the form of the Green's function appearing in the energy transmission formula. In sec. 5.3 we consider the transmission of plane waves across the system and, using two different approaches, obtain the form of the transmission coefficient. The transmission coefficient can also be expressed in terms of the same nonequilibrium Green's function and using this we write the relation between it and $\mathcal{T}(\omega)$. This relation is then used in sec. 5.4 to derive the Landauer formula for heat current. Finally we discuss our results in sec. 5.5.

Consider the set-up in Fig. (5.1) where a one-dimenional (1D) harmonic chain with arbitrary spring constants and masses is connected to leads which are themselves ordered harmonic chains. Special cases of this setup have been discussed earlier by various authors [51–56] in the context of

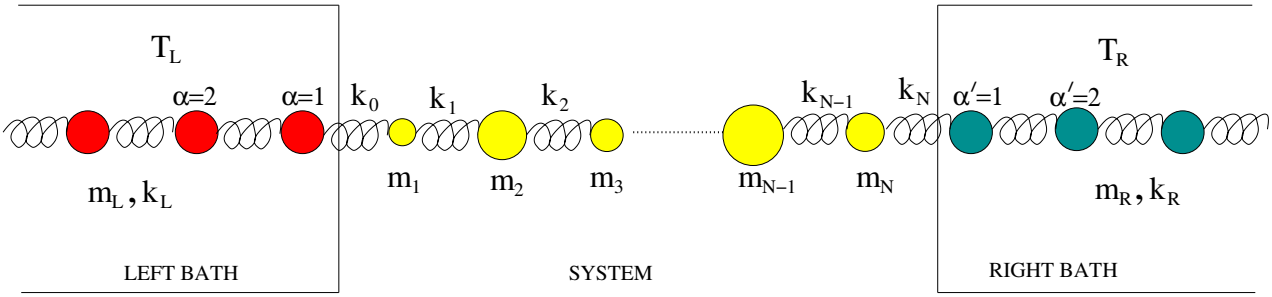

FIGURE 5.1: Schematic of the set-up considered here. The system consists of a harmonic chain of N particles for which both the particle masses and the inter-particle spring constants take arbitrary values. The system is sandwiched between two reservoirs which are ordered $1D$ harmonic chains with different mass densities and elasticities. The coupling constant between left reservoir and system is k_0 and between right reservoir and system is k_N.

heat conduction. Let us assume that the system has N Cartesian positional degrees of freedom $\{x_l\}$, $l = 1, 2 \ldots, N$ with corresponding momenta $\{p_l\}$. These satisfy the usual commutation relations $[x_l, p_m] = i\hbar\delta_{l,m}$ and $[x_l, x_m] = [p_l, p_m] = 0$. Similarly the left reservoir degrees of freedom are denoted by $\{x_\alpha, p_\alpha\}$, $\alpha = 1, \ldots, N_L$ and the right reservoirs by $\{x_{\alpha'}, p_{\alpha'}\}$, $\alpha' = 1, \ldots, N_R$. We consider our system plus reservoir to be described by the full Hamiltonian

$$\begin{aligned}\mathcal{H} &= \sum_{l=1}^{N} \frac{p_l^2}{2m_l} + \sum_{l=1}^{N-1} \frac{k_l (x_l - x_{l+1})^2}{2} \\ &+ \sum_{\alpha=1}^{N_L} \frac{p_\alpha^2}{2m_L} + \sum_{\alpha=1}^{N_L} \frac{k_L (x_\alpha - x_{\alpha+1})^2}{2} + \frac{k_0 (x_{\alpha=1} - x_1)^2}{2} \\ &+ \sum_{\alpha'=1}^{N_R} \frac{p_{\alpha'}^2}{2m_R} + \sum_{\alpha'=1}^{N_R} \frac{k_R (x_{\alpha'} - x_{\alpha'+1})^2}{2} + \frac{k_N (x_{\alpha'=1} - x_N)^2}{2} \,, \end{aligned} \tag{5.2}$$

where we assume $x_{\alpha=N_L+1} = x_{\alpha'=N_R+1} = 0$. The system masses $\{m_l\}$ and spring constants $\{k_l\}$ are assumed to be arbitrary. The left (right) reservoir particle masses are all taken to be m_L (m_R) and the inter-particle spring constants are taken to be k_L (k_R). To ensure a unique steady state We will always assume that the reservoirs are chosen to have sufficiently broad bandwidths compared to the spectrum of the system [40, 57]. The above Hamiltonian can be written in the canonical form:

$$\mathcal{H} = \mathcal{H}_S + \mathcal{H}_L + \mathcal{H}_R + \mathcal{H}_{LS} + \mathcal{H}_{RS} \,, \tag{5.3}$$

where

$$\begin{aligned}
\mathcal{H}_S &= \sum_{l=1}^{N} \frac{p_l^2}{2m_l} + \sum_{l=1}^{N-1} \frac{k_l(x_l - x_{l+1})^2}{2} + \frac{k_0 {x_1}^2}{2} + \frac{k_N {x_N}^2}{2} \ , \\
\mathcal{H}_L &= \sum_{\alpha=1}^{N_L} \frac{p_\alpha^2}{2m_L} + \frac{k_L(x_\alpha - x_{\alpha+1})^2}{2} + \frac{k_0 x_{\alpha=1}^2}{2} \ , \\
\mathcal{H}_R &= \sum_{\alpha'=1}^{N_R} \frac{p_{\alpha'}^2}{2m_R} + \frac{k_R(x_{\alpha'} - x_{\alpha'+1})^2}{2} + \frac{k_N x_{\alpha'=1}^2}{2} \ , \\
\mathcal{H}_{LS} &= -k_0 x_{\alpha=1} x_1, \qquad \mathcal{H}_{RS} = -k_N x_{\alpha'=1} x_N \ . \qquad (5.4)
\end{aligned}$$

Using the vector notation $X_S^T = (x_1, x_2, \ldots, x_N)$, $P_S^T = (p_1, p_2, \ldots, p_N)$ and similarly X_L, X_R, P_L, P_R, the different parts in the above Hamiltonian can be written as

$$\begin{aligned}
\mathcal{H}_S &= \frac{1}{2} P_S^T \ \boldsymbol{M}_S^{-1} \ P_S + \frac{1}{2} X_S^T \ \boldsymbol{K}_S \ X_S \ , \\
\mathcal{H}_L &= \frac{1}{2} {P_L}^T \ \boldsymbol{M}_L^{-1} \ P_L + \frac{1}{2} {X_L}^T \ \boldsymbol{K}_L X_L \ , \\
\mathcal{H}_R &= \frac{1}{2} {P_R}^T \ \boldsymbol{M}_R^{-1} \ P_R + \frac{1}{2} {X_R}^T \ \boldsymbol{K}_R X_R \ , \\
\mathcal{H}_{LS} &= X_S^T \ \boldsymbol{K}_{SL} \ X_L \ , \quad \mathcal{H}_{RS} = X_S^T \ \boldsymbol{K}_{SR} \ X_R \ ,
\end{aligned}$$

where $\boldsymbol{M}_S,\ \boldsymbol{M}_L,\ \boldsymbol{M}_R$ and $\boldsymbol{K}_S,\ \boldsymbol{K}_L,\ \boldsymbol{K}_R$ denote respectively the mass matrix and the force-constant matrix of the system, left reservoir and right reservoir, while $\boldsymbol{K}_{SL}$ and $\boldsymbol{K}_{SR}$ denote the linear coupling coefficients between the two reservoirs and the system. In our case $\boldsymbol{K}_{SL}$ is a $N \times N_L$ matrix whose only non-zero element is $[\boldsymbol{K}_{SL}]_{1,1} = k_0$, while $\boldsymbol{K}_{SR}$ is a $N \times N_R$ matrix whose only non-zero element is $[\boldsymbol{K}_{SR}]_{N,1} = k_N$.

Expression for steady state heat current: We now consider the situation where at some distant past time ($t < t_0$) the two reservoirs are uncoupled from the system and are separately in equilibrium (and described by canonical distributions) at temperatures T_L and T_R respectively. At time t_0 we start evolving the system plus reservoirs with the full Hamiltonian in Eq. (5.3). Eventually we set the reservoir sizes $N_L, N_R \to \infty$ and $t_0 \to -\infty$. The system reaches a nonequilibrium steady state at finite t. Note that we have included terms involving the coupling coefficients k_0, k_N in the isolated reservoir Hamiltonians. As has been discussed using various approaches [40–42], the steady state current can be expressed using the following phonon Green's

function:

$$\boldsymbol{G}^{\pm} \;=\; \frac{1}{-\boldsymbol{M}_S\omega^2 + \boldsymbol{K}_S - \boldsymbol{\Sigma}_L^{\pm} - \boldsymbol{\Sigma}_R^{\pm}}\,, \tag{5.5}$$

where the self-energies $\boldsymbol{\Sigma}_L^{\pm}, \boldsymbol{\Sigma}_R^{\pm}$ can be expressed in terms of the isolated reservoir Green functions $\mathrm{g}_L^{\pm}(\omega) = [\; -\boldsymbol{M}_L(\omega \pm i\epsilon)^2 + \boldsymbol{K}_L]^{-1}$, $\mathrm{g}_R^{\pm}(\omega) = \; [-\boldsymbol{M}_R(\omega \pm i\epsilon)^2 + \boldsymbol{K}_R]^{-1}$ and the coupling matrices $\boldsymbol{K}_{SL},\; \boldsymbol{K}_{SR}$. The self energies are given by $\boldsymbol{\Sigma}_L^{\pm}(\omega) = \boldsymbol{K}_{SL}\; \mathrm{g}_L^{\pm}(\omega)\; \boldsymbol{K}_{SL}^T,\; \boldsymbol{\Sigma}_R^{\pm}(\omega) = \boldsymbol{K}_{SR}\; \boldsymbol{g}_R^{\pm}(\omega)\; \boldsymbol{K}_{SR}^T$. Defining $\boldsymbol{\Gamma}_L(\omega) = \mathrm{Im}[\; \boldsymbol{\Sigma}_L^{+}\;]$, $\boldsymbol{\Gamma}_R(\omega) = \mathrm{Im}[\; \boldsymbol{\Sigma}_R^{+}\;]$, we find [40–42] that the steady state current is given by the formula in Eq. (5.1) with

$$\mathcal{T}(\omega) = 4Tr[\boldsymbol{G}_+(\omega)\boldsymbol{\Gamma}_L(\omega)\boldsymbol{G}_-(\omega)\boldsymbol{\Gamma}_R(\omega)]\;. \tag{5.6}$$

For our one-dimensional system, we note that $\boldsymbol{G}^{\pm}, \boldsymbol{\Sigma}_L^{\pm}, \boldsymbol{\Sigma}_R^{\pm}$ are all $N \times N$ matrices. The only non-zero elements of $\boldsymbol{\Sigma}_L^{\pm}$ and $\boldsymbol{\Sigma}_R^{\pm}$ are respectively $[\boldsymbol{\Sigma}_L^{\pm}]_{1,1} = {k_0}^2[\boldsymbol{g}_L^{\pm}]_{1,1} =: \Sigma_L^{\pm}$ and $[\boldsymbol{\Sigma}_R^{\pm}]_{N,N} = {k_N}^2[\boldsymbol{g}_R^{\pm}]_{1,1} =: \Sigma_R^{\pm}$. Let us define $\Gamma_L = Im[\Sigma_L^{+}]$, $\Gamma_R = Im[\Sigma_R^{+}]$. Hence the expression of $\mathcal{T}$ reduces to:

$$\mathcal{T} = 4\Gamma_L\Gamma_R\boldsymbol{G}_{1,N}^{+}\boldsymbol{G}_{N,1}^{-} = 4\Gamma_L\Gamma_R|\boldsymbol{G}_{1,N}^{+}|^2\;, \tag{5.7}$$

with the matrix $\boldsymbol{G}^{+} = \boldsymbol{Z}^{-1}$, where $\boldsymbol{Z} = -\boldsymbol{M}_S\omega^2 + \boldsymbol{K}_S\; - \boldsymbol{\Sigma}_L^{+} - \boldsymbol{\Sigma}_R^{+}$ is a tri-diagonal matrix. The bandwidth of the two baths are different ($2\sqrt{k_L/m_L}$ and $2\sqrt{k_R/m_R}$ for the left and right baths respectively), so the conduction of heat across the system will have contribution only from the overlapping part of the bandwidths. As shown in the Appendix below, for our one-dimensional model we can obtain the following explicit forms of Γ_L, Γ_R and $\boldsymbol{G}_{1,N}^{+}$:

$$\begin{aligned}
\Gamma_L \;&=\; -\frac{k_0^2 k_L sin(q)}{|k_0 - k_L + k_L\; e^{-iq}|^2}\;, \quad \Gamma_R = -\frac{k_N^2 k_R sin(q')}{|k_N - k_R + k_R\; e^{-iq'}|^2}\;, \\
\boldsymbol{G}_{1,N}^{+} \;&=\; \frac{1}{\begin{bmatrix} 1 & -\frac{k_0^2 e^{iq}}{k_L + (k_0 - k_L)e^{iq}} \end{bmatrix}\; \hat{T}\; \begin{bmatrix} k_N & 0 \\ 0 & 1/k_N \end{bmatrix}\; \begin{bmatrix} 1 \\ \frac{{k_N}^2 e^{iq'}}{k_R + (k_N - k_R)e^{iq'}} \end{bmatrix}}\;,
\end{aligned} \tag{5.8}$$

$$\text{where} \quad \hat{T} \equiv \prod_{l=1}^{N} \hat{T}_l \ , \qquad \hat{T}_l = \begin{bmatrix} a_l/k_l & -k_l \\ 1/k_l & 0 \end{bmatrix} \ . \tag{5.9}$$

$$a_l = k_l + k_{l-1} - m_l\omega^2, \quad l = 1, \ldots, N \ ,$$

and q,q', the wavevectors associated with frequency ω in the left and right baths respectively, are related to ω through the dispersion relations

$$\omega^2 = (2k_L/m_L)\ (1 - \cos q) = (2k_R/m_R)(1 - \cos q') \ . \tag{5.10}$$

5.3 Scattering states and transmission coefficient

For our model the equations of motion correspond to the discrete wave equation for which we can construct scattering wave solutions. We will now construct solutions that correspond to plane waves incident on the system from the reservoirs. From these solutions we will obtain the transmission coefficient. In the following we will only consider the "right-moving states" which correspond to waves that are incident from the left reservoir. The "left-moving states" can be similarly obtained.

Let us consider a chain described by the Hamiltonian of Eq. (5.2) with an infinite number of particles in both the reservoirs. The particle displacements in the chain satisfy the equations of motion

$$m_l\ddot{x}_l = -(k_{l-1} + k_l)\ x_l + k_{l-1}\ x_{l-1} + k_l\ x_{l+1} \ , \tag{5.11}$$

where $l = 1, \ldots, N$ refers to particles of the system, $l \leq 0$ refers to particles of the left reservoir (*i.e* $\alpha \geq 1$, as in the notation of Eq. 5.2), and $l \geq N + 1$ refers to particles in the right reservoir (*i.e* $\alpha' \geq 1$). We note that these equations are valid both for the quantum representation, where the variables are Heisenberg operators, and also for the classical case. Corresponding to the above equations let us construct classical wave solutions ψ_l satisfying the equations

$$m_l\ddot{\psi}_l = -(k_{l-1} + k_l)\ \psi_l + k_{l-1}\ \psi_{l-1} + k_l\ \psi_{l+1} \ . \tag{5.12}$$

In the left and right reservoirs these equations take the form of the discrete wave equations

$$\begin{aligned} \ddot{\psi}_\alpha &= (k_L/m_L)(\psi_{\alpha+1} - 2\psi_\alpha + \psi_{\alpha-1}) \qquad \text{for } \alpha > 1 \ , \\ \ddot{\psi}_{\alpha'} &= (k_R/m_R)(\psi_{\alpha'+1} - 2\psi_{\alpha'} + \psi_{\alpha'-1}) \qquad \text{for } \alpha' > 1 \ . \end{aligned}$$

These have the following plane-wave solutions,

$$\begin{aligned} \psi_\alpha(q) &= \frac{1}{(2\pi m_L)^{1/2}} \, e^{-i\omega t} \, (\, e^{-iq\alpha} + r \, e^{iq\alpha} \,) \qquad \text{for } \alpha \geq 1 \ , \\ \psi_{\alpha'}(q') &= \frac{1}{(2\pi m_L)^{1/2}} \, \tau \, e^{-i\omega t} e^{iq'\alpha'} \qquad \text{for } \alpha' \geq 1 \ , \end{aligned} \tag{5.13}$$

where the wave-vectors $q, q' \in (0, \pi)$ satisfy the dispersion relations given in Eq. (5.10) and the normalization is chosen such that for $\tau = 0$ (*i*.e no transmission) the following completeness relations are satisfied:

$$\int_0^\pi dq \ m_L \psi_\alpha^*(q) \psi_\nu(q) = \delta_{\alpha,\nu} \tag{5.14}$$

for any two points α, ν on the left bath. The solution in Eq. (5.13) corresponds to a plane wave of wave vector q, frequency ω that is incident on the system from the left side, part of this is then reflected with amplitude r, and a part transmitted across the system with amplitude τ. We shall refer to τ as the transmission coefficient and will now proceed to the calculation of this. As is well-known in quantum mechanics and wave-theory, the required scattering states can be constructed either by direct solution of the equations of motion in Eq. (5.12) or by the Lippmann-Schwinger scattering theory approach. We now present both these methods.

5.3.1 Transmission coefficient from direct solution of the the wave equation

For points on the reservoirs the plane wave solution has the form in Eq. (5.13). For $0 \leq l \leq N+1$, let us write $\psi_l(q) = s_l e^{-i\omega t}$, $l = 0, .., N+1$ where the amplitudes s_l satisfy the equations

$$m_l \omega^2 s_l = (k_{l-1} + k_l) \ s_l - k_{l-1} \ s_{l-1} - k_l \ s_{l+1} \ , \tag{5.15}$$

and it is to be understood that $l = 0, l = -1$ refer to $\alpha = 1,\ \alpha = 2$ respectively while $l = N+1,\ l = N+2$ refer to $\alpha' = 1,\ \alpha' = 2$. Hence we get the following recursion relation:

$$\begin{bmatrix} k_{l-1}s_{l-1} \\ \\ s_l \end{bmatrix} = \hat{T}_l \begin{bmatrix} k_l s_l \\ \\ s_{l+1} \end{bmatrix} , \tag{5.16}$$

where $\hat{T}_l$ is defined in Eq. (5.9). Using this recursively gives

$$\begin{bmatrix} k_{-1}s_{-1} \\ \\ s_0 \end{bmatrix} = \hat{T}_0\ \hat{T}\ \hat{T}_{N+1} \begin{bmatrix} k_{N+1}s_{N+1} \\ \\ s_{N+2} \end{bmatrix} . \tag{5.17}$$

We note that

$$\begin{bmatrix} k_{-1}s_{-1} \\ \\ s_0 \end{bmatrix} = \frac{1}{(2\pi m_L)^{1/2}} \begin{bmatrix} k_L\ (e^{-2iq} + re^{2iq}) \\ \\ (e^{-iq} + re^{iq}) \end{bmatrix} , \quad \begin{bmatrix} k_{N+1}s_{N+1} \\ \\ s_{N+2} \end{bmatrix} = \frac{1}{(2\pi m_L)^{1/2}} \begin{bmatrix} k_R e^{iq'} \\ \\ e^{2iq'} \end{bmatrix} \tau ,$$

$$\hat{T}_0 = \begin{bmatrix} k_L + k_0 - m_L\omega^2 & -k_0^2 \\ \\ 1 & 0 \end{bmatrix}, \quad \hat{T}_{N+1} = \begin{bmatrix} k_R + k_N - m_R\omega^2 & -k_R^2 \\ \\ 1 & 0 \end{bmatrix} ,$$

and hence Eq. (5.17) gives

$$\hat{T}_0\ \ \hat{T}\ \hat{T}_{N+1} \begin{pmatrix} k_R e^{iq'} \\ \\ e^{2iq'} \end{pmatrix} \tau = \begin{pmatrix} k_L e^{-2iq} \\ \\ e^{-iq} \end{pmatrix} + \begin{pmatrix} k_L e^{2iq} \\ \\ e^{iq} \end{pmatrix} r . \tag{5.18}$$

To solve for τ we multiply the above equation by the row vector $(1\ \ -k_L e^{iq})$, and this gives

$$\tau = \frac{-2ik_L \sin(q)}{(e^{iq}\ \ - k_L e^{2iq})\ \hat{T}_0\ \hat{T}\ \hat{T}_{N+1} \begin{pmatrix} k_R e^{iq'} \\ \\ e^{2iq'} \end{pmatrix}} .$$

After some simplifications and using the form of $\boldsymbol{G}^{+}_{1,N}$ given in Eq. (5.8) we obtain:

$$\tau = -\frac{2ik_L \sin(q)\ k_0 k_N e^{-i(q+q')}}{(k_0 - k_L + k_L e^{-iq})(k_N - k_R + k_R e^{-iq'})}\ \boldsymbol{G}^{+}_{1,N}\ . \tag{5.19}$$

Now using the expressions for Γ_L, Γ_R in Eq. (5.8) and comparing with the formula in Eq. (5.7) we immediately see that the energy transmittance $\mathcal{T}(\omega)$ and the transmission coefficient $\tau(\omega)$ are related as

$$\mathcal{T}(\omega) = |\tau(\omega)|^2 \frac{k_R \sin(q')}{k_L \sin(q)}\ . \tag{5.20}$$

The relation between these coefficients for the case of junction transmittance ($N = 0$) was obtained in [51], where numerical evidence for such a relationship for $N > 0$ was also presented. The physical interpretation of the above relation comes from noticing that the coefficient of $|\tau|^2$ in Eq. (5.20) is the ratio of the mass times the group velocity for plane waves in the two baths [47]. Thus the transmittance simply represents the ratio between incident and transmitted energy currents.

5.3.2 Transmission coefficient from Lippmann-Schwinger scattering approach

The Lippmann-Schwinger scattering theory approach in quantum mechanics starts by breaking up the Hamiltonian of a system into an unperturbed part and a perturbation. One then writes an exact scattering solution of the unperturbed part of the Hamiltonian and then uses this to obtain a solution of the full problem in terms of the perturbation and appropriate Green's functions. Here, using the notation of Eq. (5.3), we treat $\mathcal{H}_S + \mathcal{H}_L + \mathcal{H}_R$ as the unperturbed Hamiltonian and $\mathcal{H}_{LS} + \mathcal{H}_{RS}$ as the perturbation.

Lippmann-Schwinger theory: Let us use the notation $|\psi(q)\rangle$ to denote the state for the wave-function $\psi_l(q)$ satisfying the wave equation

$$\mathrm{M}\omega^2 |\psi(q)\rangle = \mathrm{K} |\psi(q)\rangle\,, \tag{5.21}$$

where M and K are the mass matrix and force matrix respectively of the full chain (including system and reservoirs). Using the partition of the chain into the reservoir and system parts, these

matrices have the following block structures:

$$\mathrm{M} = \begin{bmatrix} \boldsymbol{M}_S & 0 & 0 \\ 0 & \boldsymbol{M}_L & 0 \\ 0 & 0 & \boldsymbol{M}_R \end{bmatrix}, \quad \boldsymbol{K} = \begin{bmatrix} \boldsymbol{K}_S & \boldsymbol{K}_{SL} & \boldsymbol{K}_{SR} \\ \boldsymbol{K}_{SL}^T & \boldsymbol{K}_L & 0 \\ \boldsymbol{K}_{SR}^T & 0 & \boldsymbol{K}_R \end{bmatrix} \tag{5.22}$$

Breaking $\boldsymbol{K}$ into unperturbed and perturbed parts we have:

$$\begin{aligned} \boldsymbol{K} &= \boldsymbol{K}_0 + \boldsymbol{K}_1 \\ \text{where} \qquad \boldsymbol{K}_0 &= \begin{bmatrix} \boldsymbol{K}_S & 0 & 0 \\ 0 & \boldsymbol{K}_L & 0 \\ 0 & 0 & \boldsymbol{K}_R \end{bmatrix}, \quad \boldsymbol{K}_1 = \begin{bmatrix} 0 & \boldsymbol{K}_{SL} & \boldsymbol{K}_{SR} \\ \boldsymbol{K}_{SL}^T & 0 & 0 \\ \boldsymbol{K}_{SR}^T & 0 & 0 \end{bmatrix}. \end{aligned} \tag{5.23}$$

Treating $\boldsymbol{K}_1$ as a perturbation we then obtain the following scattering solution of Eq. (5.21):

$$\begin{aligned} |\psi\rangle &= |\psi^0\rangle - \mathcal{G}^+ \boldsymbol{K}_1 |\psi^0\rangle \ , \\ \text{where} \quad \mathcal{G}^+ &= [-\boldsymbol{M}(\omega + i\epsilon)^2 + \boldsymbol{K}]^{-1} \end{aligned} \tag{5.24}$$

is the Green's function for the full chain and $|\psi^0\rangle$ is a scattering solution of the unperturbed system satisfying the equation

$$\mathrm{M}\omega^2 |\psi^0(q)\rangle = \mathrm{K}_0 |\psi^0(q)\rangle \ . \tag{5.25}$$

Construction of initial state: Let us first construct the right-moving scattering states. For this we consider the particular initial state $|\psi^0\rangle$ where the left reservoir is in a normal mode with frequency ω while the system and right reservoir degrees of freedom are at rest. Thus we choose $\psi_l^0(q) = 0$ for $l > 0$ and $\psi_l^0(q) = \psi_\alpha^L$ for $l \leq 0$, with $\alpha = 1 - l$ and $\psi_\alpha^L(q)$ satisfying the equation

$$m_L \omega^2 \psi_\alpha^L(q) = \sum_\beta [\mathrm{K}_L]_{\alpha,\beta} \psi_\beta^L(q) \ . \tag{5.26}$$

The form of $\boldsymbol{K}_L$ can be read from Eq. (5.4), and we then get

$$m_L\omega^2\psi^L_\alpha(q) = k_L[\ 2\psi^L_\alpha(q) - \psi^L_{\alpha+1}(q) - \psi^L_{\alpha-1}(q)\ ] + \delta_{\alpha,1}(k_0 - k_L)\psi^L_1(q)\ , \quad \alpha = 1, 2, \ldots \tag{5.27}$$

with the boundary condition $\psi^L_0(q) = 0$. For $k_0 = k_L$ the normal modes are given by $\psi^L_\alpha(q) = 2i\sin q\alpha/(2\pi m_L)^{1/2}$, where the normalization is chosen such that $\int_0^\pi dq\ m_L{\psi^L}^*_\alpha(q)\psi^L_\nu(q) = \delta_{\alpha,\nu}$. For $k_0 \neq k_L$ we can find the normal modes by treating the last term in Eq. (5.27) as a perturbation. We will require only $\psi^L_{\alpha=1}(q)$. The Lippmann-Schwinger approach is applied again, giving

$$\psi^L_{\alpha=1}(q) = \frac{2i\ \sin(q)}{(2\pi m_L)^{1/2}}\ \left[1 - (k_0 - k_L)\ [\mathrm{g}^+_L]_{1,1}\right] = -\frac{2i\ \sin q}{(2\pi m_L)^{1/2}}\ k_L e^{-iq}\ [\mathrm{g}^+_L]_{1,1}, \tag{5.28}$$

where the result in Eq. (5.47) has been used. Note that our choice of ψ^L_0 implies an incident wave $e^{iq\alpha}/(2\pi m_L)^{1/2}$.

Scattering state: Since we want to finally find τ, it is sufficient to compute the scattering wave function only on the right reservoir. From Eq. (5.24) we get

$$\psi_{\alpha'}(q) = -\mathcal{G}^+_{\alpha',l=1}k_0\psi^L_{\alpha=1}(q)\ . \tag{5.29}$$

We now express the Green's function element $-\mathcal{G}^+_{\alpha',l=1}$ in terms of the Green's function $\boldsymbol{G}^+$ defined earlier in Eq. (5.5). We first write $\mathcal{G}^+$ in a block-matrix form, with the different blocks representing the system and reservoirs. This matrix satisfies the following relation:

$$\begin{bmatrix} -\boldsymbol{M}^S(\omega+i\epsilon)^2 + \boldsymbol{K}_S & \boldsymbol{K}_{SL} & \boldsymbol{K}_{SR} \\ \boldsymbol{K}_{SL}{}^T & -\boldsymbol{M}^L\ (\omega+i\epsilon)^2 + \boldsymbol{K}_L & 0 \\ \boldsymbol{K}_{SR}{}^T & 0 & -\boldsymbol{M}^R\ (\omega+i\epsilon)^2 + \boldsymbol{K}_R \end{bmatrix} \times \begin{bmatrix} \boldsymbol{G}^+_S & \boldsymbol{G}^+_{SL} & \boldsymbol{G}^+_{SR} \\ \boldsymbol{G}^+_{LS} & \boldsymbol{G}^+_L & \boldsymbol{G}^+_{LR} \\ \boldsymbol{G}^+_{RS} & \boldsymbol{G}^+_{RL} & \boldsymbol{G}^+_R \end{bmatrix} = \begin{bmatrix} \boldsymbol{I} & 0 & 0 \\ 0 & \boldsymbol{I} & 0 \\ 0 & 0 & \boldsymbol{I} \end{bmatrix}\ . \tag{5.30}$$

From this equation the following relations can be shown to hold [40]:

$$\boldsymbol{G}_S^+(\omega) = \frac{1}{-\omega^2 \boldsymbol{M}^S + \boldsymbol{K}_S - \boldsymbol{\Sigma}_L^+ - \boldsymbol{\Sigma}_R^+} =: \boldsymbol{G}^+(\omega) \ , \tag{5.31}$$

$$\boldsymbol{G}_{RS}^+ = \mathrm{g}_R^+ \boldsymbol{K}_{SR} \boldsymbol{G}^+ \ . \tag{5.32}$$

This then gives us

$$\mathcal{G}^+_{\alpha',l=1} = [\boldsymbol{G}^+_{RS}]_{\alpha',l=1} = [\mathrm{g}_R^+]_{\alpha',1} k_N \boldsymbol{G}^+_{N,1} \ . \tag{5.33}$$

Using Eqs. (5.28,5.33) in Eq. (5.29) we finally get:

$$\psi_{\alpha'}(q') = 2ik_0 k_N k_L \sin q e^{-iq} [\mathrm{g}_L^+]_{1,1} [\mathrm{g}_R^+]_{\alpha',1} \boldsymbol{G}^+_{1,N} / (2\pi m_L)^{1/2} \ . \tag{5.34}$$

Now taking the $(\alpha', 1)^{\mathrm{th}}$ element of Eq. (5.46), with L replaced by R, and using Eq. (5.48) we get

$$[\mathrm{g}_R^+]_{\alpha',1} = \frac{e^{iq'\alpha'}}{k_R + (k_N - k_R)e^{iq'}} \ . \tag{5.35}$$

Using the explicit form of $[\mathrm{g}_L^+]_{1,1}$ from Eq. (5.47) we finally arrive at the expected form of the transmitted wave function in the right reservoir

$$\psi_{\alpha'}(q') = \tau e^{iq'\alpha'} / (2\pi m_L)^{1/2}$$

with τ precisely given by the same expression Eq. (5.19) obtained in the previous sub-section by the direct solution of the wave equation.

5.4 Expression for the energy current in each mode and a derivation of the Landauer formula

We now use the definition of the heat current operator and show how it can be used to express the current contribution of each of the modes in terms of the transmission coefficient and hence the energy transmittance. This will lead us to a derivation of the Landauer formula. In the steady state the current is constant everywhere and we will evaluate it on the right reservoir. Between sites α' and $\alpha'+1$ the left-right current is given by the expectation value [11] $\hat{j}_L = \langle \, \frac{1}{2} k_R (v_{\alpha'} + v_{\alpha'+1})(x_{\alpha'} -$

$x_{\alpha'+1})\rangle$ where we compute the average using the $q^{\rm th}$ right-moving state obtained in the previous section. It is easiest to obtain this using second-quantized notation. The set of right moving and left moving states form a complete set. Denoting the left-movers by $\psi_{\alpha'}(q)$ with $q \in (-\pi, 0)$ we note that they satisfy the completeness relation $\int_{-\pi}^{\pi} dq (m_{\alpha'})^{1/2}(m_{\nu'})^{1/2}\psi^*_{\alpha'}(q)\psi_{\nu'}(q) = \delta_{\alpha',\nu'}$. The displacement and velocity operators at the lattice sites of the right bath can be expressed in terms of the creation and annihilation operators $a_{q'}, a^\dagger_{q'}$ as

$$\begin{aligned} x_{\alpha'} &= \int_{-\pi}^{\pi} dq \left(\frac{\hbar}{2\omega_q}\right)^{\frac{1}{2}} \left[a_q\psi_{\alpha'}(q) + a^\dagger_q{\psi_{\alpha'}}^*(q)\right] \ , \\ v_{\alpha'} &= -i\int_{-\pi}^{\pi} dq \left(\frac{\hbar\omega_q}{2}\right)^{\frac{1}{2}} \left[a_q\psi_{\alpha'}(q) - a^\dagger_q{\psi_{\alpha'}}^*(q)\right] \ . \end{aligned}$$

The operators $a_{q_1}, a^\dagger_{q_2}$ satisfy the commutation relations $[a_{q_1}, a^\dagger_{q_2}] = \delta(q_1 - q_2)$ and, using the completeness relation, it can be verified that this ensures the usual commutation relations for the position and momentum operators. Using the above we get for the expectation value of the current for a right moving state:

$$\begin{aligned} J_{LR}(q) &= i\hbar k_R(\langle a^\dagger_q a_q\rangle + \frac{1}{2})[{\psi_{\alpha'+1}}^*(q)\psi_{\alpha'}(q) - \psi_{\alpha'+1}(q){\psi_{\alpha'}}^*(q)] \\ &= \frac{\hbar k_R \sin(q')}{\pi m_L}\ |\tau|^2\ [f(\omega_q, T_L) + \frac{1}{2}] \ , \end{aligned} \tag{5.36}$$

where in the last step we have used the form $\psi_{\alpha'}(q) = \tau e^{i\alpha' q'}/(2\pi m_L)^{1/2}$, and the initial occupation probability of the state q is given by the left bath thermal distribution $\langle a^\dagger_q a_q\rangle = [e^{\hbar\omega_q/k_B T_L} - 1]^{-1} = f(\omega, T_L)$. The total current transmitted from the left bath to the right bath, is obtained by integrating over all q. After making a change of variables from q to $\omega = 2(k_L/m_L)^{1/2}\sqrt{1-\cos(q)}$ we get

$$\begin{aligned} J_{LR} &= \int_0^{\pi} dq J_{LR}(q) \\ &= \frac{1}{\pi}\int_0^{2(k_L/m_L)^{1/2}} d\omega\ \hbar\omega \frac{k_R\sin(q')}{k_L \sin q}\ |\tau|^2\ [f(\omega, T_L) + \frac{1}{2}] \\ &= \frac{1}{\pi}\int_0^{2(k_L/m_L)^{1/2}} d\omega\ \hbar\omega\mathcal{T}(\omega)\ [f(\omega, T_L) + \frac{1}{2}] \ , \end{aligned} \tag{5.37}$$

where in the last step we used Eq. (5.20) . From symmetry, the current flowing from the right bath to the left bath will be given by

$$J_{RL} = \frac{1}{\pi}\int_0^{2(k_R/m_R)^{1/2}} d\omega\ \hbar\omega\mathcal{T}(\omega)\ [f(\omega, T_R) + \frac{1}{2}] \ .$$

Hence finally we get for the net current:

$$J = \frac{1}{\pi}\int_0^{\omega_m} d\omega \hbar\omega \mathcal{T}(\omega)[f(\omega, T_L) - f(\omega, T_R)] \ , \tag{5.38}$$

where $\omega_m = \min[2(k_L/m_L)^{1/2}, 2(k_R/m_R)^{1/2}]$. Observing that $\mathcal{T}$ is a symmetric function of ω and vansishes outside the range $\omega \in (0, \omega_m)$, we can see that Eq. (5.38) is equivalent to the Landauer formula Eq. (5.1) .

5.5 Discussion

In summary we have studied heat conduction across a $1D$ quantum-mechanical harmonic chain, with arbitrary distribution of masses and inter-particle spring constants, that is connected to two other ordered $1D$ harmonic crystals which have different mass densities and elastic constants. For this model we use two different approaches to demonstrate the relation $\mathcal{T}(\omega) = (k_R \sin q')\ |\tau(\omega)|^2/(k_L \sin q)$ between the energy transmittance $\mathcal{T}(\omega)$, which occurs in the Landauer formula for heat current, and the transmission coefficient $\tau(\omega)$ related to passage of plane waves across the system. In the first approach we use the fact that the Green's function occuring in the expression for $\mathcal{T}$ has a simple representation in terms of product of 2×2 matrices. The plane wave solutions are then obtained by directly solving the equations of motion and a representation of τ is obtained, again in terms of the product of matrices. The connection between $\mathcal{T}$ and τ is then directly obtained. This approach can be extended to the case of regular lattices using, for example, the techniques used in [58] for the representation of the Green's functions using matrix products.

In the second approach it is not necessary to find the explicit form of the Green's function. One notes that the required plane wave scattering states can be obtained by using the Lippmann-Schwinger approach to evolve initial states which are eigenmodes of either one of the reservoirs and are initially localized within the reservoirs. The Lippmann-Schwinger approach then directly gives τ in terms of the Green's function. This second approach is more powerful since it can be used for arbitrary harmonic structures where it is not possible to think of simple plane wave scattering states. This approach tells us that we need to construct scattering states by evolving the eigenmodes of the two isolated reservoirs. Indeed this is what the NEGF approach does in effect

and our explicit calculations for a simple but representative model clarifies the picture. Our exact calculations also illustrate some of the subtle points involved, such as the correct computation of the self-energies Σ_L^+, Σ_R^+ for inhomogeneous chains, appropriate normalizations of normal-modes and the choice of initial states.

APPENDIX

Explicit forms for $\boldsymbol{G}_{1,N}^+, \Gamma_L, \Gamma_R$: Using methods described in [2] we now show that the Green's function element occuring in Eq. (5.7) can be expressed in terms of a product of 2×2 matrices. We also obtain the explicit forms of Γ_L, Γ_R for our particular model. The matrix $\boldsymbol{Z}$ has the form

$$\boldsymbol{Z}(\omega) = \begin{bmatrix} a_1 - \Sigma_L^+(\omega) & -k_1 & \cdots & 0 & 0 & 0 \\ -k_1 & a_2 & -k_2 & \cdots & 0 & 0 \\ \vdots & \vdots & \vdots & \ddots & \vdots & \vdots \\ 0 & 0 & \cdots & -k_{N-2} & a_{N-1} & -k_{N-1} \\ 0 & 0 & 0 & \cdots & -k_{N-1} & a_N - \Sigma_R^+(\omega) \end{bmatrix}, \quad (5.39)$$

$$\text{where } a_l = k_l + k_{l-1} - m_l\omega^2, \quad l = 1, \ldots, N \ .$$

Taking the inverse of this matrix, we get

$$\boldsymbol{G}_{1,N}^+ = \frac{\prod_{l=1}^{N-1} k_l}{\Delta_{1,N}} \ , \quad (5.40)$$

where $\Delta_{1,N}$ is defined as the determinant of the matrix $\boldsymbol{Z}(\omega)$. Let us also define $D_{l,j}$ as the determinant of the sub-matrix starting with the l-th row and column and ending with the j-th row and column of the matrix $-\boldsymbol{M}_S\omega^2 + \boldsymbol{K}_S$. From the tri-diagonal form of the matrices, it is

easily shown that

$$\begin{aligned}\Delta_{1,N} &= (\ a_1 - \Sigma_L^+\ )\ [\ (a_N - \Sigma_R^+)\ D_{2,N-1} - k_{N-1}D_{2,N-2}\ ] - k_1\ [\ (a_N - \Sigma_R^+)D_{3,N-1} - k_{N-1}D_{3,N-2}\ ] \\ &= D_{1,N} - \Sigma_R^+ D_{1,N-1} - \Sigma_L^+ D_{2,N} + \Sigma_L^+\Sigma_R^+ D_{2,N-1} \\ &= \begin{bmatrix} 1 & -\Sigma_L^+ \end{bmatrix} \begin{bmatrix} D_{1,N} & -D_{1,N-1} \\ D_{2,N} & -D_{2,N-1} \end{bmatrix} \begin{bmatrix} 1 \\ \Sigma_R^+ \end{bmatrix} . \end{aligned} \tag{5.41}$$

The elements $D_{l,j}$ satisfy the recursion relation $D_{l,N} = a_l D_{l+1,N} - k_l^2 D_{l+2,N}$ for $l = 1, ...N-2$, and $D_{l,N-1} = a_l D_{l+1,N-1} - k_l^2 D_{l+2,N-1}$ for $l = 1, ...N-3$. In matrix form these give

$$\begin{bmatrix} D_{l,N} & -D_{l,N-1} \\ D_{l+1,N} & -D_{l+1,N-1} \end{bmatrix} = k_l \begin{bmatrix} a_l/k_l & -k_l \\ 1/k_l & 0 \end{bmatrix} \begin{bmatrix} D_{l+1,N} & -D_{l+1,N-1} \\ D_{l+2,N} & -D_{l+2,N-1} \end{bmatrix} , \tag{5.42}$$

which holds for $l = 1, ...N-3$. Using the easily computed values of $D_{N-1,N-1}$, $D_{N,N-1}$, $D_{N-1,N}$, and $D_{N,N}$, we arrive at the result

$$\begin{bmatrix} D_{1,N} & -D_{1,N-1} \\ D_{2,N} & -D_{2,N-1} \end{bmatrix} = \prod_{l=1}^{N} k_l\ \hat{T} \begin{bmatrix} 1 & 0 \\ 0 & 1/{k_N}^2 \end{bmatrix} , \tag{5.43}$$

(5.44)

where $\hat{T}$ is defined in (5.9).

Hence using Eqs. (5.41,5.43) we get

$$\Delta_{1,N} = (\prod_{l=1}^{N} k_l) \begin{bmatrix} 1 & -\Sigma_L^+ \end{bmatrix} \hat{T} \begin{bmatrix} 1 & 0 \\ 0 & 1/k_N^2 \end{bmatrix} \begin{bmatrix} 1 \\ \Sigma_R^+ \end{bmatrix} . \tag{5.45}$$

We next find the explicit forms of Σ_L^+, Σ_R^+, for which we need to evaluate the reservoir Green's function elements $[\mathrm{g}_L^+]_{1,1}$ and $[\mathrm{g}_R^+]_{1,1}$. Consider the left reservoir. For the case $k_0 = k_L$, it is

simple to find all normal modes and hence compute the Green's function corresponding to the force matrix $\boldsymbol{K}_L = \boldsymbol{K}_L^0$ (say). One gets

$$\begin{aligned} \mathrm{g}_L^{0+} &= \frac{1}{-\boldsymbol{M}_L\,(\omega+i\epsilon)^2 + \boldsymbol{K}_L^0} \\ \text{Hence}\;\; [\mathrm{g}_L^{0+}]_{l,m} &= \frac{2}{m_L\pi}\int_0^\pi dq \frac{\sin(ql)\sin(qm)}{-(\omega+i\epsilon)^2+\Omega_q^2}\ , \\ \text{where}\;\; \Omega_q^2 &= \frac{2k_L}{m_L}[1-\cos(q)]\ . \end{aligned}$$

We need the $(1,1)^{\text{th}}$ element and the above integral gives $[\mathrm{g}_L^{0+}]_{1,1} = e^{iq}/k_L$, where q is to be obtained from $\omega^2 = (2k_L/m_L)(1-\cos q)$. For the general case $k_0 \neq k_L$, the Green's function can be calculated as follows. We write $\boldsymbol{K}_L = \boldsymbol{K}_L^0 + \Delta\boldsymbol{K}_L$ where $\Delta\boldsymbol{K}_L$ is a perturbartion matrix whose the only non-zero element is $\Delta\boldsymbol{K}_{11} = k_0 - k_L$. From the definition of the Green's function $\mathbf{g}_{\boldsymbol{L}}^+ = [-\boldsymbol{M}_L(\omega+i\epsilon)^2 + \boldsymbol{K}_L^0 + \boldsymbol{\Delta K}_L]^{-1}$ we get

$$\boldsymbol{g}_L^+ + \boldsymbol{g}_L^{0+}\boldsymbol{\Delta K}_L\boldsymbol{g}_L^+ = \boldsymbol{g}_L^{0+}\ . \tag{5.46}$$

Taking the $(1,1)^{\text{th}}$ element of the above equation gives

$$[\mathrm{g}_L^+]_{1,1} = \frac{[\mathrm{g}_L^{0+}]_{11}}{1+[\mathrm{g}_L^{0+}]_{11}\;[\boldsymbol{\Delta K}_L]_{11}} = \frac{e^{iq}}{k_L+(k_0-k_L)e^{iq}}\ , \tag{5.47}$$

and similarly

$$[\mathrm{g}_R^+]_{1,1} = \frac{e^{iq'}}{k_R+(k_N-k_R)e^{iq'}}\ . \tag{5.48}$$

Using the definitions given earlier we derive the following expressions:

$$\begin{aligned} \Sigma_L^+ &= \frac{k_0^2 e^{iq}}{k_L+(k_0-k_L)e^{iq}}, \quad \Sigma_R^+ = \frac{k_N^2 e^{iq'}}{k_R+(k_N-k_R)e^{iq'}}, \\ \Gamma_L &= -\frac{k_0^2 k_L sin(q)}{|k_0-k_L+k_L\;e^{-iq}|^2}, \quad \Gamma_R = -\frac{k_N^2 k_R sin(q')}{|k_N-k_R+k_R\;e^{-iq'}|^2}\ , \end{aligned} \tag{5.49}$$

where q, q' are respectively obtained from the relations $\omega^2 = (2k_L/m_L)(1-\cos q) = (2k_R/m_R)(1-\cos q')$ and Γ_L, Γ_R are non-zero only when both q, q' are real. Plugging in the expressions of Σ_L^+ and Σ_R^+ in Eq. (5.45), we obtain from Eq. (5.40) the final result of Eq. (5.8).

References

[1] Z. Rieder, J. L. Lebowitz, E. Lieb, J. Math. Phys. **8**, 1073 (1967).

[2] A. Casher, J. L. Lebowitz, J. Math. Phys. **12**, 1701 (1971.)

[3] H. Matsuda and K. Ishii, Prog. Theor. Phys. Suppl. **45**, 56 (1970)

[4] O. Narayan and S. Ramaswamy, Phys. Rev. Lett. **89**, 200601 (2002).

[5] S. Lepri, R. Livi, and A. Politi, Phys. Rev. Lett. 78, 1896 (1997).

[6] H. van Beijeren, Phys. Rev. Lett. **108** , 180601 (2012).

[7] H. Spohn, J. Stat. Phys. **154**, 1191 (2014).

[8] Y. Zhong, Y. Zhang, J. Wang, H. Zhao, Phys. Rev. E **85**, 060102(R) (2012).

[9] S. Chen, Y. Zhang, J. Wang, H. Zhao, **arXiv:1204.5933**.

[10] S. Lepri, R. Livi, and A. Politi, Phys. Rev. Lett. 78, 1896 (1997); A. Dhar, Phys. Rev. Lett. **88**, 249401 (2002); P. Grassberger, W. Nadler, and L. Yang, Phys. Rev. Lett. **89**, 180601 (2002); G. Casati and T. Prosen, Phys. Rev. E **67**, 015203 (2003); P. Cipriani, S. Denisov, and A. Politi, Phys. Rev. Lett. **94**, 244301 (2005); T. Mai, A. Dhar and O. Narayan, Phys. Rev. Lett. **98**, 184301 (2007); J. M. Deutsch and O. Narayan, Phys. Rev. E **68**, 010201(R) (2003).

[11] A. Dhar, Adv. Phys. **57**, 457 (2008).

[12] M. P. Allen and D. L. Tildesley, *Computer Simulations of Liquids* (Clarendon, Oxford, 1987).

[13] J. M. Deutsch and O. Narayan, Phys. Rev. E **68**, 041203 (2003).

[14] A. Kundu, A. Dhar, and O. Narayan, J. Stat. Mech. (2009) L03001.

[15] S. Chen, Y. Zhang, J. Wang, H. Zhao, arXiv:1208.0888.

[16] C. B. Mendl, H. Spohn, Phys. Rev. E **90**, 012147 (2014).

[17] L. Delfini, S. Lepri, R. Livi, A. Politi, Phys. Rev. E **73**, 060201 (2006).

[18] O. Narayan and S. Ramaswamy, Phys. Rev. Lett. **89**, 200601 (2002).

[19] J. S. Wang and B. Li, Phys. Rev. Lett. **92**, 074302 (2004).

[20] A. Pereverzev, Phys. Rev. E **68** 056124 (2003).

[21] J. Lukkarinen and H. Spohn, Commun. Pure Appl. Math. **61** 1753-1786 (2008).

[22] G. Basile, C. Bernardin and S. Olla, Phys. Rev. Lett.,**96** 204303 (2006).

[23] H. Zhao, Phys. Rev. Lett. **96** 140602 (2006).

[24] S. Chen, Y. Zhang, J. Wang and H. Zhao, arXiv:1106.2896v2 (2011).

[25] P. Cipriani, S. Denisov, and A. Politi, Phys. Rev. Lett. **94**, 244301 (2005).

[26] V. Zaburdaev, S. Denisov, and P. Hänggi, Phys. Rev. Lett. **106**, 180601 (2011).

[27] S. Lepri and A. Politi, Phys. Rev. E **83** 030107 (2011).

[28] A. Dhar, K. Saito and B. Derrida Phys. Rev. E **87**, 010103(R) (2013).

[29] S. Liu, P. Hänggi, N. Li, J. Ren and B. Li, Phys. Rev. Lett. **112**, 040601 (2014).

[30] M. Prähofer, H. Spohn, J. Stat. Phys. 115, 255 (2004).

[31] M. Prähofer, http://www-m5.ma.tum.de/KPZ.

[32] S. G. Das, A. Dhar, O. Narayan, J. Stat. Phys. **154**, 204 (2014).

[33] S.-i. Sasa, Phys. Rev. Lett. **112**, 100602 (2014).

[34] C. Giardina, R. Livi, A. Politi, and M. Vassali, Phys. Rev. Lett. **84**, 2144 (2000).

[35] O. V. Gendelman, A. V. Savin, Phys. Rev. Lett. **84**, 2381 (2000).

[36] Y. Li, S. Liu, N. Li, P. Hanggi and B. Li, arXiv:1407.1161v2.

[37] L. Yang, P. Grassberger, arXiv:cond-mat/0306173

[38] C. Bernardin, V. Kannan, J. L. Lebowitz, J. Lukkarinen, J. Stat. Phys. **146**, 800 (2012)

[39] D.E. Angelescu, M.C. Cross, M.L. Roukes, Superlattices Microsctruc. **23**, 673 (1998); L.G.C. Rego and G. Kirczenow, Phys. Rev. Lett. **81** 232 (1998); M.P. Blencowe, Phys. Rev. B **59**, 4992 (1999).

[40] A. Dhar and D. Roy, J. Stat Phys. **125**, 801 (2006).

[41] J.-S. Wang, J. Wang and N. Zeng, Phys. Rev. B **74**, 033408 (2006).

[42] T. Yamamoto and K. Watanabe, Phys. Rev. Lett. **96**, 255503 (2006).

[43] Y. Imry and R. Landauer, Rev. Mod. Phys. **71**, S306 (1999).

[44] C. Caroli et al., J. Phys. C **4**, 916 1971; Y. Meir and N. S. Wingreen, Phys. Rev. Lett. **68**, 2512 1992; A. Dhar and D. Sen, Phys. Rev. B **73**, 085119 (2006).

[45] T. N. Todorov, G. A. D. Briggs and A. P. Sutton, J. Phys.: Condens. Matter **5**, 2389 (1993).

[46] P. A. Khomyakov, G. Brocks, V. Karpan, M. Zwierzycki, and P.J. Kelly, Phys. Rev. B **72**, 035450 (2005).

[47] J.-S. Wang, J. Wang, and J. T. Lü, Eur. Phys. J. B **62**, 381 (2008).

[48] Y. A. Kosevich, Phys. Rev. B **52**, 1017(1995).

[49] N. Mingo and Liu Yang, Phys. Rev. B **68**, 245406 (2003).

[50] M. A. Panzer and K. E. Goodson, J. Appl. Phys. **103**, 094301 (2008).

[51] L. Zhang, P. Keblinski, J. S. Wang and B. Li, Phys. Rev. B **83**, 064303 (2011).

[52] R. J. Rubin and W. L. Greer, J. Math. Phys. **12**, 1686 (1971).

[53] H. Spohn and J. L. Lebowitz, Commun. math. Phys. **54**, 97 (1977).

[54] M. E. Lumpkin, W. M. Saslow, W. M. Visscher, Phys. Rev. B **17**, 4295 (1978).

[55] D. Segal, A. Nitzan, P. Hanggi, Jn. Chem. Phys. **119**, 6840 (2003).

[56] A. Dhar, K. Saito and P. Hanggi, Phys. Rev. E **85**, 011126 (2012).

[57] A. Dhar and D. Sen, Phys. Rev. B **73**, 085119 (2006).

[58] A. Chaudhuri, A. Kundu, D. Roy, A. Dhar, J. L. Lebowitz, and H. Spohn, Phys. Rev. B **81**, 064301 (2010).